

## THE 2140 $\text{cm}^{-1}$ (4.673 MICRONS) SOLID CO BAND: THE CASE FOR INTERSTELLAR $\text{O}_2$ AND $\text{N}_2$ AND THE PHOTOCHEMISTRY OF NONPOLAR INTERSTELLAR ICE ANALOGS

JAMIE ELSILA,<sup>1</sup> LOUIS J. ALLAMANDOLA,<sup>2</sup> AND SCOTT A. SANDFORD<sup>2</sup>

NASA Ames Research Center, MS 245-6, Moffett Field, CA 94035

Received 1996 June 6; accepted 1996 October 31

### ABSTRACT

The infrared spectra of CO frozen in nonpolar ices containing  $\text{N}_2$ ,  $\text{CO}_2$ ,  $\text{O}_2$ , and  $\text{H}_2\text{O}$  and the UV photochemistry of these interstellar/precometary ice analogs are reported. The spectra are used to test the hypothesis that the narrow 2140  $\text{cm}^{-1}$  (4.673  $\mu\text{m}$ ) interstellar absorption feature attributed to solid CO might be produced by CO frozen in ices containing nonpolar species such as  $\text{N}_2$  and  $\text{O}_2$ . It is shown that mixed molecular ices containing CO,  $\text{N}_2$ ,  $\text{O}_2$ , and  $\text{CO}_2$  provide a good match to the interstellar band at all temperatures between 12 and 30 K both before and after photolysis. The optical constants (real and imaginary parts of the index of refraction) in the region of the solid CO feature are reported for several of these ices. The  $\text{N}_2$  and  $\text{O}_2$  absorptions at 2328  $\text{cm}^{-1}$  (4.296  $\mu\text{m}$ ) and 1549  $\text{cm}^{-1}$  (6.456  $\mu\text{m}$ ), respectively, are also shown.

The best matches between the narrow interstellar band and the feature in the laboratory spectra of nonpolar ices are for samples which contain comparable amounts of  $\text{N}_2$ ,  $\text{O}_2$ ,  $\text{CO}_2$ , and CO. Co-adding the CO band from an  $\text{N}_2:\text{O}_2:\text{CO}_2:\text{CO} = 1:5:\frac{1}{2}:1$  ice with that of an  $\text{H}_2\text{O}:\text{CO} = 20:1$  ice provides an excellent fit across the *entire* interstellar CO feature. The four-component, nonpolar ice accounts for the narrow 2140  $\text{cm}^{-1}$  portion of the feature which is associated with quiescent regions of dense molecular clouds. Using this mixture, and applying the most recent cosmic abundance values, we derive that between 15% and 70% of the available interstellar N is in the form of frozen  $\text{N}_2$  along several lines of sight toward background stars. This is reduced to a range of 1%–30% for embedded objects with lines of sight more dominated by warmer grains. The cosmic abundance of O tied up in frozen  $\text{O}_2$  lies in the 10%–45% range toward background sources, and it is between 1% and 20% toward embedded objects. The amount of oxygen tied up in CO and  $\text{CO}_2$  frozen in nonpolar ices can be as much as 2%–10% toward background sources and on the order of 0.2%–5% for embedded objects. Similarly 3%–13% of the carbon is tied up in CO and  $\text{CO}_2$  frozen in nonpolar ices toward field stars, and 0.2%–6% toward embedded objects. These numbers imply that most of the N is in  $\text{N}_2$ , and a significant fraction of the available O is in  $\text{O}_2$  in the most quiescent regions of dense clouds.

Ultraviolet photolysis of these ices produces a variety of photoproducts including  $\text{CO}_2$ ,  $\text{N}_2\text{O}$ ,  $\text{O}_3$ ,  $\text{CO}_3$ , HCO,  $\text{H}_2\text{CO}$ , and possibly NO and  $\text{NO}_2$ . XCN is not produced in these experiments, placing important constraints on the origin of the enigmatic interstellar XCN feature.  $\text{N}_2\text{O}$  and  $\text{CO}_3$  have not been previously considered as interstellar ice components.

*Subject headings:* dust, extinction — ISM: abundances — ISM: lines and bands — ISM: molecules

### 1. INTRODUCTION

CO is the most abundant diatomic interstellar molecule after  $\text{H}_2$ . Following its discovery in the interstellar gas by Wilson, Jefferts, & Penzias in 1971, CO quickly became the most studied of gas-phase interstellar molecules. Indeed, it has proved to be a powerful diagnostic of conditions in a wide variety of astronomical environments and has given great insight into structure on a galactic scale (Latter et al. 1996). Although the possibility that CO might also be frozen on interstellar grains and in comets has been postulated for some time (see Herzberg 1955; Ewing, Thompson, & Pimentel 1960), the serious study of interstellar *solid* state CO had a slow start.

The discovery of infrared absorption in the vicinity of the feature now attributed to CO frozen on grains was made by Soifer et al. (1979) in the spectrum of the embedded protostar W33 A. Due to insufficient resolution, and the fact (then unknown) that this region of the spectrum of W33 A is

dominated by the XCN band centered at 2165  $\text{cm}^{-1}$  (4.619  $\mu\text{m}$ ), the authors reasoned that the absorption probably arose from CO, either in the gas or solid state, but they could not account for the apparent peak shift with respect to the expected position of about 2140  $\text{cm}^{-1}$  (4.673  $\mu\text{m}$ ). The first comparison between this spectrum (and the spectra of other embedded objects) with the spectrum of an interstellar ice analog containing CO was made by Hagen, Allamandola, & Greenberg (1980). In discussing the interstellar spectra, they pointed out that, “The very important null gap (missing *Q* branch) region between 2135 and 2140  $\text{cm}^{-1}$  is not yet available at very high resolution. It is difficult to overemphasize the importance of this region because the mid-infrared spectrum of a heterodiatom molecule such as CO is very different depending on whether or not the molecule is in the gas or solid phase.” This ultimately led to the first high-resolution observations of W33 A in this spectral region and the clear-cut detection of CO frozen on interstellar grains by Lacy et al. (1984). The observations showed that the low-resolution feature in W33 A detected by Soifer et al. consisted of three bands: a strong, very broad absorption at 2165  $\text{cm}^{-1}$  (4.619  $\mu\text{m}$ , FWHM = 28

<sup>1</sup> Current address: 1411 Three Mile, Grosse Pointe Park, MI 48230.

<sup>2</sup> NASA Ames Research Center, MS 245-6, Moffett Field, CA 94035-1000.

cm<sup>-1</sup>), a weak narrow band at 2140 cm<sup>-1</sup> (4.673 μm, FWHM = 5 cm<sup>-1</sup>), and an even weaker, broad feature at 2135 cm<sup>-1</sup> (4.684 μm, FWHM = 12 cm<sup>-1</sup>). (These FWHM are the full-width at half-maximum of the bands when plotted in absorbance, or optical depth.) Based on comparisons with the spectra of laboratory analogs, Lacy et al. showed that the 2135 and 2140 cm<sup>-1</sup> bands arise from solid CO, and that the 2165 cm<sup>-1</sup> band was due to the CN stretch in an unidentified species designated XCN.

Following this work, the study of solid state interstellar CO began in earnest. Over the next few years the CO feature was detected along several lines of sight through the Taurus dark cloud (Whittet, Longmore, & McFadzean 1985; Whittet et al. 1989) and toward a number of protostellar objects embedded in dense clouds (Geballe 1986). Taken together, these observations showed that (i) the 2135 and 2140 cm<sup>-1</sup> bands were both evident in the spectra of many clouds, (ii) the amount of solid CO varied with respect to other interstellar ice components such as H<sub>2</sub>O, and (iii) the spectra of some embedded objects did not show any solid state CO absorption.

During this same period, laboratory spectral analysis of CO-containing ices (Sandford et al. 1988) led to the following conclusions: (i) the broad 2135 cm<sup>-1</sup> band is most likely due to CO frozen in an H<sub>2</sub>O-rich ice with an H<sub>2</sub>O:CO ratio greater than 5, (ii) the narrower 2140 cm<sup>-1</sup> band could not be due to CO intimately mixed with H<sub>2</sub>O or any other polar ice species likely to be important in molecular clouds, and (iii) the narrower band could be matched by CO frozen in certain nonpolar ices. Of these ices studied by Sandford et al., those dominated by CO<sub>2</sub> provided the best fits to the interstellar 2140 cm<sup>-1</sup> feature. That some of the interstellar CO was frozen in nonpolar ice came as something of a surprise since the 3250 cm<sup>-1</sup> (3.08 μm) H<sub>2</sub>O ice feature dominated the infrared spectra of dense clouds, leading to the belief that H<sub>2</sub>O was the major component of interstellar ices.

By 1989, however, evidence was starting to mount that more CO was frozen in nonpolar ices than in polar, H<sub>2</sub>O-rich ices. The 2140 cm<sup>-1</sup> CO band toward SVS (CK 20) in the Serpens molecular cloud measured by Eiroa & Hodapp (1989) was much stronger than the broader 2135 cm<sup>-1</sup> feature corresponding to CO frozen in H<sub>2</sub>O. Band depth analysis implied an H<sub>2</sub>O/CO column density ratio of 2.86, making CO the second most abundant mantle material along this line of sight. This was also the first case in which the peak optical depth of the 2140 cm<sup>-1</sup> CO band exceeded the depth of the very strong 3250 cm<sup>-1</sup> H<sub>2</sub>O ice feature. Thorough subsequent observations and analysis of the frozen CO feature along many lines of sight by Tielens et al. (1991) and Chiar et al. (1994, 1995) now make it clear that the 2140 cm<sup>-1</sup> band dominates the 2135 cm<sup>-1</sup> component along most lines of sight through quiescent regions of dense clouds. Based on the laboratory data of Sandford et al. (1988), Chiar et al. (1994, 1995) showed that a significant fraction (~40%) of the total CO abundance is found frozen in the nonpolar ices, with the solid CO column density typically being ~30% that of H<sub>2</sub>O along these same lines of sight. In contrast, no more than a few percent of the available CO is frozen onto the grains along the lines of sight toward embedded protostars such as W33 A (6%; Mitchell, Allen, & Maillard 1988; Mitchell et al. 1990) where most of the frozen CO is in the polar, H<sub>2</sub>O-rich ices that produce the 2135 cm<sup>-1</sup> band.

Recent reviews of these observations in the context of a general overview of interstellar molecular ices have been given by Whittet (1993) and Sandford (1996a, 1996b). Other laboratory studies which provide data that are of relevance for interstellar CO ice include a study of the binding energies and vaporization properties of frozen CO (Sandford & Allamandola 1990a), the temperature behavior of the 2135 cm<sup>-1</sup> band due to CO in H<sub>2</sub>O ice (Schmitt, Greenberg, & Grim 1989), the behavior of the infrared band of frozen CO as a function of ion irradiation and temperature (Palumbo & Strazzulla 1993), the optical constants for CO frozen in a number of mixtures (Hudgins et al. 1993, 1994), and band strengths refined to an accuracy of a few percent for the solid CO band of pure CO and CO frozen in a number of mixtures (Gerakines et al. 1995).

Despite the great amount of lab work and the ever increasing number of astronomical spectra, the exact identity of the solid matrix that produces the narrow CO absorption at 2140 cm<sup>-1</sup> has remained uncertain. Sandford et al. (1988) showed that, of the nonpolar ice constituents considered in their extensive laboratory study, CO frozen in a CO<sub>2</sub>-rich ice came closest to matching the interstellar band position. Using this laboratory data, Eiroa & Hodapp (1989), Tielens et al. (1991), Kerr, Adamson, & Whittet (1991), and Chiar et al. (1994, 1995) have shown that most of the interstellar features could be matched by co-adding the profiles of CO<sub>2</sub>:CO, H<sub>2</sub>O:CO, and O<sub>2</sub>:CO ices, with the best fits requiring co-adding different amounts of ices with differing ratios for different objects.

While the matches to the 2140 cm<sup>-1</sup> band are reasonably good, they are not perfect and several doubts remain. For example, invoking varying amounts of three different binary ices seems somewhat contrived. Furthermore, the laboratory spectra do not reproduce the interstellar band profile in detail, especially on the high-frequency side. In addition, comparisons of laboratory spectra of CO in CO<sub>2</sub> with astronomical observations are satisfactory only over a limited temperature range (Tielens et al. 1991) and at high concentrations of CO<sub>2</sub> (CO<sub>2</sub>/CO = 20). It is difficult to understand how so much CO<sub>2</sub> could be present. Models of interstellar chemistry cannot account for the large amount needed (Tielens & Hagen 1982; d'Hendecourt, Allamandola, & Greenberg 1985). The limited observations which are available for CO<sub>2</sub> also suggest that the abundance of frozen CO<sub>2</sub> is roughly equal to that of solid CO along those lines of sight which have some contribution from quiescent regions (d'Hendecourt & Jourdain de Muizon 1989). Orbital infrared telescopes equipped with spectrometers capable of resolving the CO<sub>2</sub> bands such as the recently launched *Infrared Space Observatory (ISO)* will certainly place important further constraints on the amount of CO<sub>2</sub> frozen on interstellar grains.

Since there are some doubts regarding CO<sub>2</sub>-rich ices, other suggestions for possible origins of this feature have been considered. These include pure frozen CO, and CO-rich ices containing H<sub>2</sub>O at a H<sub>2</sub>O/CO ratio of about 1/10 (Tielens et al. 1991), and ion irradiated pure CO and mixed molecular ices (Palumbo & Strazzulla 1993). While the suggestion of pure CO ices seems unlikely due to the amount of other species available in the interstellar medium, CO-rich mixtures, ion irradiated or not, are plausible. Indeed, our studies of UV irradiated H<sub>2</sub>O-rich mixed molecular ices also shift the frozen CO feature into close agreement to the 2140 cm<sup>-1</sup> position. However, these radi-

ation processes should be less important in the quiescent regions of clouds characterized by the  $2140\text{ cm}^{-1}$  band than toward protostellar regions where the  $2135\text{ cm}^{-1}$  band is more important.

In view of these questions, we have studied the CO band in ices containing various mixtures of CO, N<sub>2</sub>, O<sub>2</sub>, CO<sub>2</sub>, and H<sub>2</sub>O in an attempt to understand the origin of the narrow  $2140\text{ cm}^{-1}$  interstellar absorption band. The three nonpolar species N<sub>2</sub>, O<sub>2</sub>, and CO<sub>2</sub> have been chosen because theoretical models of interstellar ice grain chemistry have long predicted that these species are important in certain dense cloud environments (Tielens & Hagen 1982; d'Hendecourt et al. 1985). Furthermore, the definitive detection of NH<sub>3</sub> (ice), long considered as a likely repository of interstellar N, has been elusive (Whittet et al. 1996; Sandford & Allamandola 1993). We have also investigated the photolysis of these ices, as photochemical studies of nonpolar interstellar ice analogs are quite scarce.

In the following section (§ 2), we briefly discuss the experimental techniques used in this study. The spectroscopic data and photochemical results are presented in § 3 along with the optical constants (real and imaginary parts of the index of refraction—*n*'s and *k*'s) across the solid CO band for several relevant interstellar ice analogs. In § 4 we compare these results to astronomical data and conclude that interstellar ices made up of N<sub>2</sub>, O<sub>2</sub>, and CO<sub>2</sub> are plausible. The astrophysical implications of these results are discussed in § 5, including the implied N<sub>2</sub> and O<sub>2</sub> interstellar abundances and depletions, and the new interstellar grain species suggested by the photolysis experiments. The main conclusions are summarized in § 6.

## 2. EXPERIMENTAL METHODS

Only a brief summary will be given here, since the general procedures used have been described elsewhere (Allamandola, Sandford, & Valero 1988; Sandford et al. 1988). Glass bulbs containing the gas mixtures to be studied were prepared in a greaseless, glass vacuum system. Gas samples (CO, Matheson C.P., 99.5% purity; CO<sub>2</sub>, Matheson Bone Dry, 99.8% purity; O<sub>2</sub>, Matheson Extra Dry, 99.6% purity) were introduced into the glass vacuum line directly from lecture bottles without further purification. N<sub>2</sub> (Aircro Dry, 99.9% purity) was introduced into the sample preparation line only after passage through a liquid nitrogen cooled trap. H<sub>2</sub>O (triply distilled) was further purified by three freeze-pump-thaw cycles before use. Once prepared, each mixture was allowed to equilibrate overnight.

After transferring the bulb to the cryogenic sample preparation system, the mixture was then deposited under vacuum onto a cold ( $\sim 12\text{ K}$ ) CsI substrate. The deposition rate was typically between  $10^{-2}$  and  $10^{-1}$  moles  $\text{hr}^{-1}$ .

Deposition times for these experiments ranged from 2 s to 30 minutes. The infrared spectrum of the resulting amorphous ice was then recorded using a Fourier transform infrared spectrometer. All spectra are presented here in percent transmittance and the FWHM listed in the tables correspond to percent transmittance, not optical depth or absorbance. Spectral resolution is  $0.9\text{ cm}^{-1}$  (the width of an unresolved line) and band positions are accurate to  $\pm 0.2\text{ cm}^{-1}$  due to oversampling. Subsequently, the ice was warmed in steps to higher temperatures, and the infrared spectrum recorded at each temperature.

Previous studies utilizing inert gas matrices and mixed molecular ices have shown that the substrate (CsI in this case) has no discernible effect on the absorption spectrum of the ice as measured here. While the first few layers in contact with the substrate are presumably affected, measuring an IR absorption spectrum requires several thousand molecular layers. It has been shown that epitaxial effects are negligible compared to the bulk interactions within the ice itself which determine the position and profile of the spectral feature (see, e.g., Sandford et al. 1988).

Ultraviolet photolysis of several mixtures was carried out using a microwave-powered hydrogen flow lamp. An H<sub>2</sub>:He = 1:9 gas mixture was used in the photolysis lamp. This enhances the  $1216\text{ \AA}$  Lyman- $\alpha$  line emission relative to general continuum emission. The ices were kept at 12 K during the irradiation periods, which were typically about 3 hr. In cases where the samples were photolyzed, the spectrum was recorded before and after irradiation as well as during warm-up.

## 3. EXPERIMENTAL RESULTS

Table 1 presents a summary of all the mixtures examined as part of this study. Entries in parentheses indicate the mixtures that were photolyzed. The results are presented as follows. First, the frozen CO band profile dependence on concentration in binary N<sub>2</sub>:CO mixtures is described in § 3.1.1. Second, the influence of H<sub>2</sub>O on the CO peak position and profile in N<sub>2</sub>:H<sub>2</sub>O:CO ices is discussed in § 3.1.2. Third, the effects of the presence of other molecules such as CO<sub>2</sub> and O<sub>2</sub> on the solid CO feature with and without N<sub>2</sub> are considered in § 3.1.3. Lastly, four component ices comprised of N<sub>2</sub>:O<sub>2</sub>:CO<sub>2</sub>:CO are described in § 3.1.4. In all cases, the CO band temperature dependence was also studied. The photochemistry of a few of the ices is described in § 3.2, and the optical constants of a number of the ice mixtures studied here are presented in § 3.3. Finally, the bands produced by solid N<sub>2</sub> and O<sub>2</sub> are discussed briefly in § 3.4.

All measurements of peak positions and widths presented in the tables were made from the original spectra. However,

TABLE 1  
CO-CONTAINING ICES CONSIDERED IN THIS STUDY<sup>a</sup>

Molecules	Relative Concentrations
N <sub>2</sub> :CO .....	(100:1), 25:1, (2:1), (1:20)
O <sub>2</sub> :CO .....	20:1
CO <sub>2</sub> :CO .....	20:1
N <sub>2</sub> :H <sub>2</sub> O:CO .....	100:1:1, (19:1:1), 10:1:1, 5:1:1, (2:1:1), 5:1:5, 10:1:10
N <sub>2</sub> :O <sub>2</sub> :CO .....	(1:1:1), 1:5:1
N <sub>2</sub> :CO <sub>2</sub> :CO .....	1:1:1, 1:5:1
N <sub>2</sub> :O <sub>2</sub> :CO <sub>2</sub> :CO .....	1:3:5:1, 1:5:3/2:1, (1:5:1/2:1)

<sup>a</sup> Mixtures in parentheses were also photolyzed.

the baselines were flattened for the figures in those cases where the spectra showed significant tilts or curvature, or contained strong interference fringes. All spectra are presented in percent transmittance and the FWHM listed in the tables correspond to percent transmittance plots, not optical depth or absorbance. The data are plotted in this way since this permits a better assessment of the fit across the entire feature.

### 3.1. The Frozen CO Feature in Nonpolar Ices

#### 3.1.1. N<sub>2</sub>:CO Ices

A series of mixed-molecular ices having different N<sub>2</sub>:CO concentrations were studied. The N<sub>2</sub> to CO ratios were chosen to bracket plausible interstellar ratios associated with a range of possible environments. The spectra of these ices were measured at 12 K and at several temperatures up to 35 K. The profiles of the CO bands are shown in Figure 1 and peak positions and widths are listed in Table 2. Values are given in the table only at those temperatures where a measurable, reproducible change occurred in position or width during warm up. Figure 2 shows the change in the CO profile that occurs upon warm-up of the N<sub>2</sub>:CO = 1:20 ice. The sudden shift in position, increase in width, and decrease in strength above ~30 K listed in Table 2 for the N<sub>2</sub>:CO = 25:1 and 2:1 ices corresponds to the temperatures at which the nitrogen softens and begins to sublime, releasing much of the trapped CO. The profile of the CO band is broader because it is in a much less rigid, more irregular cage.

#### 3.1.2. N<sub>2</sub>:H<sub>2</sub>O:CO Ices

Since H<sub>2</sub>O is an abundant interstellar ice constituent, a series of ices containing N<sub>2</sub>, CO, and H<sub>2</sub>O were also prepared and studied. The relative amounts of each component were varied in order to be able to bracket a wide range of H<sub>2</sub>O concentrations in the ices. Ices dominated by H<sub>2</sub>O were not considered here since they have been discussed elsewhere (see Sandford et al. 1988). The CO bands produc-

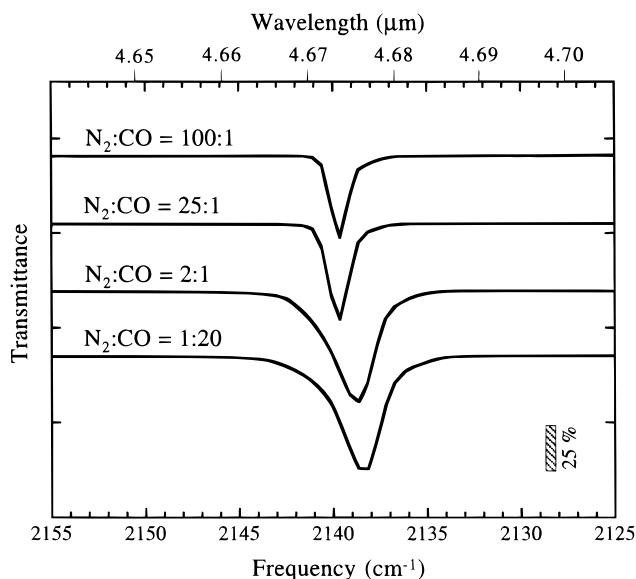


FIG. 1.—The concentration dependence of the CO band in N<sub>2</sub>:CO ices at 12 K. All spectra are plotted on the scale indicated by the bar in the lower right side of the figure. The spectra are offset vertically from each other for clarity.

TABLE 2

PEAK POSITIONS AND FWHM OF THE CO FEATURE IN N<sub>2</sub>:CO ICES AS A FUNCTION OF TEMPERATURE<sup>a</sup>

Ice Temperature	CO Position (cm <sup>-1</sup> )	FWHM (cm <sup>-1</sup> )
N <sub>2</sub> :CO = 100:1		
12 K.....	2139.6	1.1
25 K.....	2139.6	1.0
32 K.....	2139.6	1.1
N <sub>2</sub> :CO = 25:1		
12 K.....	2139.7	1.2
30 K.....	2139.7	1.3
33 K.....	2137.8	~8
N <sub>2</sub> :CO = 2:1		
12 K.....	2138.7	2.6
30 K.....	2138.7	2.5
32 K.....	2138.7	2.3
34 K.....	2140.1	~8
N <sub>2</sub> :CO = 1:20		
12 K.....	2138.2	2.6
25 K.....	2138.2	2.3
32 K.....	2138.7	2.0
34 K.....	2139.2	7.0

<sup>a</sup> All ices deposited at 12 K and then warmed to the indicated temperatures.

ed by these ices are shown in Figure 3, with band positions and FWHM listed in Table 3. In many of these ices a second band appeared near 2148 cm<sup>-1</sup> (see also Sandford et al. 1988; Schmitt et al. 1989; Palumbo & Strazzulla 1993). This feature has been attributed to a second CO trapping site in amorphous H<sub>2</sub>O ices (Sandford et al. 1988). These

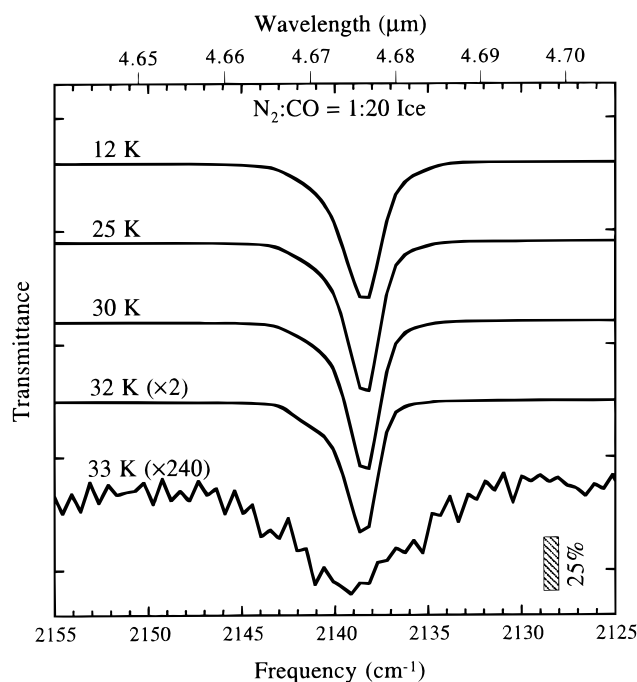


FIG. 2.—The temperature dependence of the CO band in a N<sub>2</sub>:CO = 1:20 ice. All spectra are plotted on the scale indicated by the bar in the lower right side of the figure. The spectra are offset vertically from each other for clarity.

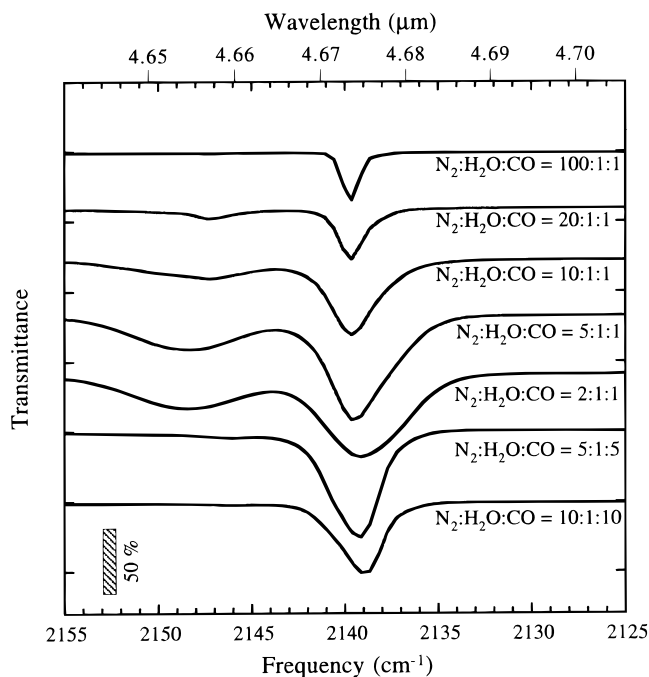


FIG. 3.—The concentration dependence of the CO band in  $N_2:H_2O:CO$  ices at 12 K. All spectra are plotted on the scale indicated by the bar in the lower left side of the figure. The spectra are offset vertically from each other for clarity. The extra feature peaking near  $2148\text{ cm}^{-1}$  in several mixtures is induced by the presence of  $H_2O$ .

data suggest that the second site is characterized by a dangling OH bond which forms a weak complex with the CO. Positions and widths for this second band are listed in parentheses in Table 3. Sandford et al. (1988) and Schmitt et al. (1989) have studied the temperature behavior of the 2148 and  $2135\text{ cm}^{-1}$  bands. See Jenniskens et al. (1995) for further discussion of these sites.

### 3.1.3. $O_2:CO$ , $CO_2:CO$ , $N_2:O_2:CO$ , and $N_2:CO_2:CO$ Ices

Since the  $2140\text{ cm}^{-1}$  feature is indicative of CO in a nonpolar ice, binary mixtures of CO in  $O_2$  and  $CO_2$  were studied to compare with the  $N_2$ -containing ices since these species are also likely to be abundant in quiescent regions of dense molecular clouds (Tielens & Hagen 1982; d'Hendecourt et al. 1985). Several ternary mixtures containing CO with  $N_2$  and  $O_2$ , or  $N_2$  and  $CO_2$  were also investigated. The results of these experiments are listed in Table 4 and shown in Figures 4 and 5.

### 3.1.4. $N_2:O_2:CO_2:CO$ Ices

Comparison of the spectra presented in § 3.1.1 to § 3.1.3 with interstellar spectra shows that combinations of binary and ternary ices containing CO with  $N_2$ ,  $O_2$ , and  $CO_2$  are required to produce a band consistent with the interstellar feature. Consequently, a few four-component ices containing  $N_2$ ,  $O_2$ ,  $CO_2$ , and CO were also studied. The results of these experiments are listed in Table 4 and shown in Figure 6.

## 3.2. Photochemistry

The UV photochemistry of the seven ice mixtures listed in parentheses in Table 1 was also studied. The infrared spectra of the mixtures taken after UV photolysis were com-

TABLE 3  
PEAK POSITIONS AND FWHM OF THE CO FEATURE IN  $N_2$ - AND  $H_2O$ -CONTAINING MIXED-MOLECULAR ICES<sup>a,b</sup>

Ice Temperature	CO Position ( $\text{cm}^{-1}$ )	FWHM ( $\text{cm}^{-1}$ )
$N_2:H_2O:CO = 100:1:1$		
12 K .....	2139.6 (2148.4)	1.2 (1.2)
25 K .....	2139.7 (2146.9)	0.9 (1.4)
30 K .....	2139.6 (2146.9)	1.1 (1.3)
35 K .....	2141.1 (2152.5)	10.0 (8.3)
$N_2:H_2O:CO = 20:1:1$		
12 K .....	2139.6 (2147.4)	1.6 (2.3)
25 K .....	2139.6 (2149.7)	1.4 (4.0)
30 K .....	2139.6 (2150.7)	1.4 (5.3)
35 K .....	2139.6 (2150.7)	1.3 (6.7)
40 K .....	2136.2 (2151.8)	11.0 (15.0)
$N_2:H_2O:CO = 10:1:1$		
12 K .....	2139.7 (2147.3)	3.0 (7.0)
25 K .....	2139.7 (2147.4)	2.4 (7.4)
30 K .....	2139.5 (2147.3)	2.4 (7.8)
35 K .....	2138.8 (2150.1)	10.0 (7.0)
$N_2:H_2O:CO = 5:1:1$		
12 K .....	2139.6 (2148.4)	3.6 (7.2)
25 K .....	2139.6 (2148.8)	3.5 (7.2)
30 K .....	2139.2 (2149.8)	3.4 (8.0)
35 K .....	2138.3 (2149.7)	7.4 (>10)
$N_2:H_2O:CO = 2:1:1$		
12 K .....	2139.2 (2148.4)	5.3 (7.2)
25 K .....	2139.2 (2148.8)	5.3 (7.2)
30 K .....	2139.2 (2149.2)	4.8 (7.0)
35 K .....	2138.2 (2149.3)	8.5 (8.0)
$N_2:H_2O:CO = 5:1:5$		
12 K .....	2139.1 (2148.8)	4.7 (5.4)
25 K .....	2139.1 (2148.8)	4.0 (5.4)
30 K .....	2138.7 (2148.8)	4.0 (5.4)
35 K .....	2139.1 (2150.0)	9.0 (4.7)
$N_2:H_2O:CO = 10:1:10$		
12 K .....	2139.1	2.8
25 K .....	2138.7	2.8
30 K .....	2138.7	2.7
35 K .....	2138.6	~10

<sup>a</sup> Numbers in parentheses correspond to the weaker feature on the high-frequency side of the main feature (see Fig. 3).

<sup>b</sup> All ices deposited at 12 K and then warmed to the indicated temperatures.

pared with preirradiation spectra to identify photoproducts and to monitor the effect of photolysis on the solid CO feature. As an example, the  $2000\text{--}500\text{ cm}^{-1}$  ( $5\text{--}20\text{ }\mu\text{m}$ ) spectrum of the  $N_2:O_2:CO = 1:1:1$  ice is shown both before and after photolysis in Figure 7. Photolysis for periods longer than 3 hr did not produce further significant spectral changes. Four types of ices were irradiated:  $N_2:CO$  mixtures,  $N_2:H_2O:CO$  mixtures, an  $N_2:O_2:CO$  mixture, and an  $N_2:O_2:CO_2:CO$  mixture. The photoproducts and their relative abundances varied, depending on the initial ice composition. The bands due to the photoproducts from two different ices are shown in Figures 8 and 9. Identifications of the new features appearing upon photolysis are listed in Table 5. Table 6 compares the peak positions and FWHM of the CO feature before and after photolysis for all seven mixtures.

Most of the photochemistry is driven by reactions with "hot" O atoms liberated by photolysis of O<sub>2</sub>, H<sub>2</sub>O, or CO (Figs. 8 and 9). The principal species produced from O atom reactions are CO<sub>2</sub>, N<sub>2</sub>O, O<sub>3</sub>, and CO<sub>3</sub>. CO<sub>2</sub> is detected in all cases, and N<sub>2</sub>O in most. As the concentration of CO decreases (especially in the N<sub>2</sub>:CO series of ices), N<sub>2</sub>O production is favored over CO<sub>2</sub> production. Conversely, an increase in CO concentration in the N<sub>2</sub>:CO series of experiments does not favor the appearance of any other new photoproducts except CO<sub>2</sub>. Ozone appears as a photoproduct in all the mixtures, although the amount produced is highly variable. Relatively little O<sub>3</sub> is produced in the N<sub>2</sub>:CO and N<sub>2</sub>:H<sub>2</sub>O:CO ices, probably due to the lower availability of photolytic oxygen atoms present in the starting mixtures. The N<sub>2</sub>:O<sub>2</sub>:CO and N<sub>2</sub>:O<sub>2</sub>:CO<sub>2</sub>:CO ices show the strongest ozone production as measured by the strength of the 1037 cm<sup>-1</sup> (9.643 μm) ozone band. Here, enough ozone is produced that even the weaker 2108, 1104, and 704 cm<sup>-1</sup> (4.744, 9.058, and 14.20 μm) O<sub>3</sub> bands are evident. Again, this result is expected as copious "hot" O atoms are produced by the photolysis of O<sub>2</sub> under these conditions. The "hot" O atoms readily combine with undissociated O<sub>2</sub> molecules to produce O<sub>3</sub>. Photolysis of the molecular oxygen-containing ices also produced carbon trioxide (CO<sub>3</sub>), presumably by the addition of O to CO<sub>2</sub>.

The liberation of hydrogen in the H<sub>2</sub>O-containing mixtures produces the formyl radical (HCO), which appeared in low concentration in both H<sub>2</sub>O-containing mixtures, and formaldehyde (H<sub>2</sub>CO), which was detected only in the more H-rich N<sub>2</sub>:CO:H<sub>2</sub>O = 2:1:1 ice. Since formaldehyde requires the addition of one more hydrogen atom than the formyl radical, it is not surprising that it appears only when the H<sub>2</sub>O concentration is high. Several other weak features appeared between 1900 and 1750 cm<sup>-1</sup> (5.26 and 5.71 μm) in the H<sub>2</sub>O containing ices. These presumably arise from various hydrogenated forms of CO and CO<sub>2</sub> such as HOCO (Milligan & Jacox 1971).

There is some evidence for the production of NO<sub>2</sub> and NO, but it is inconclusive. NO<sub>2</sub> absorbs at 1610 cm<sup>-1</sup> in an argon matrix, at 1612 cm<sup>-1</sup> in an O<sub>2</sub> matrix (St. Louis & Crawford 1965), and at 1617 cm<sup>-1</sup> in a N<sub>2</sub> matrix (Lucas & Pimentel 1979). Thus, the band which appears near 1607 cm<sup>-1</sup> after photolysis of several ices may arise from NO<sub>2</sub>, but one would expect it to fall closer to the 1612 or 1617 cm<sup>-1</sup> positions since the mixed molecular ice environment is closer to that of solid O<sub>2</sub> or N<sub>2</sub> rather than solid Ar. Similarly, NO absorbs at 1875 cm<sup>-1</sup> in Ar and at 1883 cm<sup>-1</sup> in CO<sub>2</sub> matrices, respectively (Fateley, Bent, & Crawford 1959). Sharp, very, very weak absorptions appear at 1875 and 1860 cm<sup>-1</sup> upon photolysis of the N<sub>2</sub>:CO = 100:1 and 2:1 ices, respectively, and a sharp, weak absorption appears near 1860 cm<sup>-1</sup> in the N<sub>2</sub>:H<sub>2</sub>O:CO = 2:1:1 ice. Again, the new band falls more than 20 cm<sup>-1</sup> lower than the position expected based on the published matrix isolation studies. Furthermore, if the 1607 cm<sup>-1</sup> band is due to NO and the 1875 or 1860 cm<sup>-1</sup> absorptions are due to NO<sub>2</sub>, some correlation between these two features would be expected. However, none is seen in this limited set of data. Thus, while the spectra are suggestive of NO<sub>2</sub> and NO production, doubts remain.

### 3.3. Optical Constants ( $n + ik$ )

The real and imaginary parts of the indices of refraction

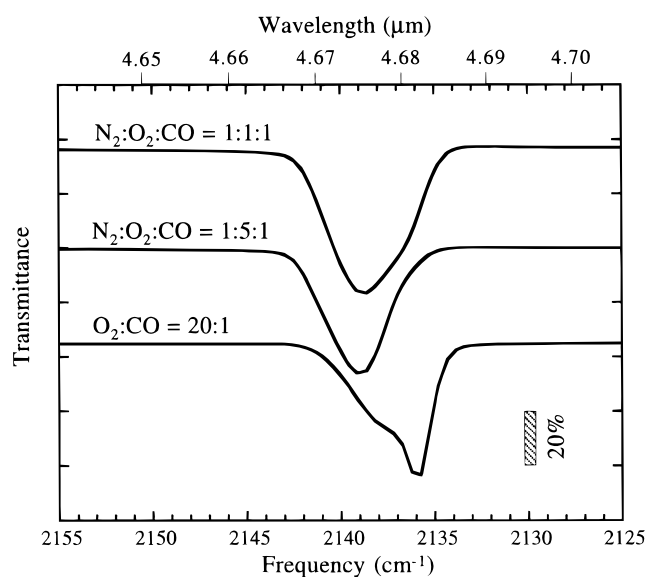


FIG. 4.—The CO band produced by several O<sub>2</sub>:CO and N<sub>2</sub>:O<sub>2</sub>:CO ices at 12 K. All spectra are plotted on the scale indicated by the bar in the lower right side of the figure. The spectra are offset vertically from each other for clarity.

( $n$  and  $k$ ) were determined for a number of the ices studied using a Kramers-Kronig analysis (Bergmen et al. 1978) of the transmission spectra. The procedure was essentially that used by Hudgins et al. (1993) to determine the optical constants of a wide variety of mixed molecular ices of astrophysical interest (see also Hudgins et al. 1994). Readers interested in the details of the calculation of the optical constants should see Hudgins et al. (1993).

Briefly, the computational procedure used to determine the complex index of refraction was as follows. Assuming a starting value for  $n [= n_0 = n_{(Na D)}]$  at all frequencies, a

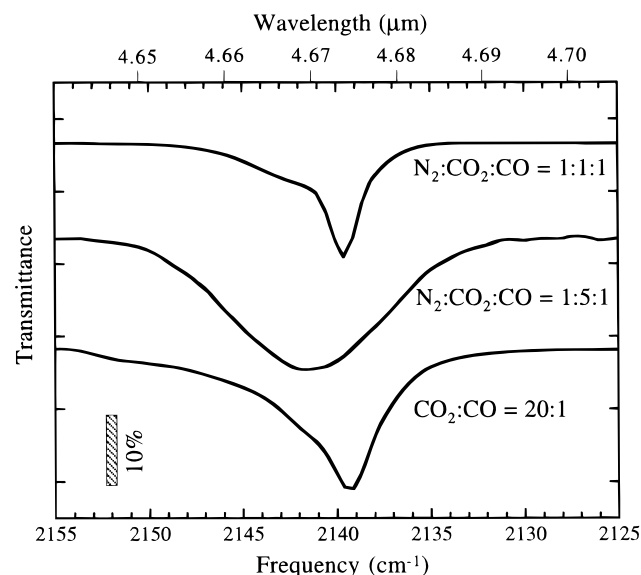


FIG. 5.—The CO band produced by several CO<sub>2</sub>:CO and N<sub>2</sub>:CO<sub>2</sub>:CO ices at 12 K. All spectra are plotted on the scale indicated by the bar in the lower left side of the figure. The spectra are offset vertically from each other for clarity.

TABLE 4  
PEAK POSITIONS AND FWHM OF THE CO FEATURE IN O<sub>2</sub>- AND CO<sub>2</sub>- CONTAINING  
MIXED-MOLECULAR ICES WITH AND WITHOUT N<sub>2</sub><sup>a</sup>

Ice Composition	Ice Temperature	CO Position (cm <sup>-1</sup> )	FWHM (cm <sup>-1</sup> )
N <sub>2</sub> :O <sub>2</sub> :CO = 1:1:1 .....	12 K	2139.2	4.0
	25 K	2139.2	3.7
	30 K	2138.7	3.3
	35 K	2138.2	6.0
N <sub>2</sub> :O <sub>2</sub> :CO = 1:5:1 .....	12 K	2138.7	3.9
	25 K	2139.2	4.2
	30 K	2139.2	3.6
	35 K	2138.7	2.7
O <sub>2</sub> :CO = 20:1 .....	12 K	2135.8	3.7
	25 K	2136.3	3.2
	30 K	2136.3	2.3
	35 K	2139.6	2.7
N <sub>2</sub> :CO <sub>2</sub> :CO = 1:1:1 .....	12 K	2139.6	2.3
	25 K	2139.6	2.3
	30 K	2139.6	2.5
	35 K	2139.7	7.4
	40 K	2140.7	8.4
	70 K	2139.6	8.0
N <sub>2</sub> :CO <sub>2</sub> :CO = 1:5:1 .....	12 K	2141.5	9.6
	25 K	2141.6	9.3
	30 K	2141.6	9.3
	35 K	2141.6	9.2
	70 K	2139.6	7.6
CO <sub>2</sub> :CO = 20:1 .....	12 K	2139.2	4.8
	35 K	2139.2	5.0
	50 K	2139.2	4.2
N <sub>2</sub> :O <sub>2</sub> :CO <sub>2</sub> :CO = 1:3:5:1 .....	12 K	2142.7	8.5
	12 K	2142.1	6.9
N <sub>2</sub> :O <sub>2</sub> :CO <sub>2</sub> :CO = 1:5:1.5:1 .....	20 K	2142.1	6.9
	25 K	2142.3	6.3
	30 K	2142.5	6.3
	35 K	2143.4	8.4
	35 K	2143.2	8.1

<sup>a</sup> All ices deposited at 12 K and then warmed to the indicated temperatures.

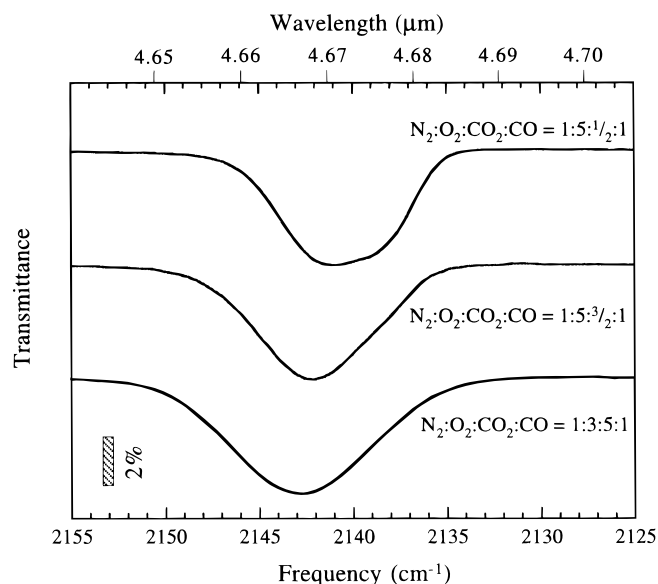


FIG. 6.—The CO band produced by several N<sub>2</sub>:O<sub>2</sub>:CO<sub>2</sub>:CO ices at 12 K. All spectra are plotted on the scale indicated by the bar in the lower left side of the figure. The spectra are offset vertically from each other for clarity.

Kramers-Kronig analysis was used to calculate the absorption coefficient and the imaginary part of the refractive index across the spectral region of interest. The real part of the refractive index was then computed. The resultant  $n$  and  $k$  values were used to compute a synthetic spectrum which was, in turn, compared to the real spectrum. Differences between the real and computed spectrum were then used to adjust the previously assumed  $n$  values. This iterative process was repeated, using the new  $n$  values generated from the previous step, until the calculated transmission spectrum differed nowhere from the measured value by more than 0.1%. The number of iterations required to fulfill this requirement depended on the number, strength, and width of the absorption features within the spectrum. For the spectra discussed here, the number of iterations required typically fell between 10 and 30, although spectra dominated by strong, narrow bands like those produced by CO<sub>2</sub> occasionally required almost 100. The correct operation of the program was initially verified by comparing our results against values already reported in the literature. Our technique gives good agreement with those reported for H<sub>2</sub>O (Bertie, Labbe, & Whalley 1969; Hagen, Tielens, & Greenberg 1981; Leger et al. 1983), CO<sub>2</sub> (Wood & Roux 1982; Warren 1986), CO (Roux et al. 1980), and CH<sub>4</sub> (Roux

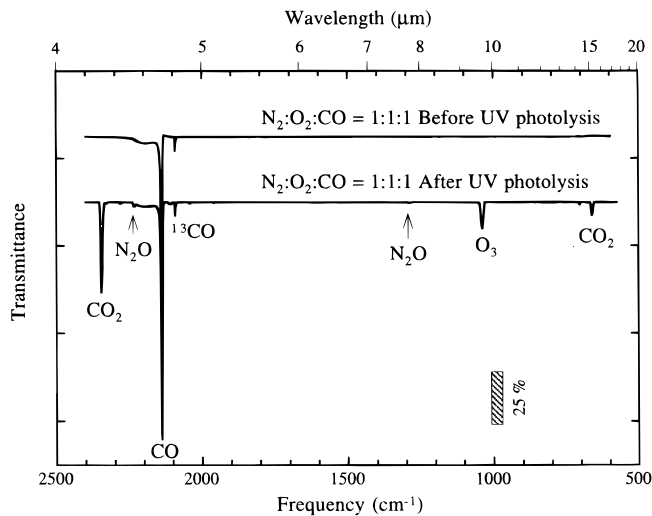


FIG. 7.—The spectrum of an N<sub>2</sub>:O<sub>2</sub>:CO = 1:1:1 ice at 12 K before (upper trace) and after (lower trace) 3 hr of UV photolysis.

et al. 1980; Pearl et al. 1991).

For ices dominated by N<sub>2</sub> and O<sub>2</sub>, where CO produced the only absorption band of any significance, calculations were carried out only over the 2250–2050 cm<sup>-1</sup> (4.44–4.88 μm) region using all the data points in the experimental

spectrum in this interval (corresponding to ~1 point every 0.5 cm<sup>-1</sup>). Ices containing CO<sub>2</sub> and H<sub>2</sub>O, however, produce additional absorption features that must be accounted for. In these cases, the calculations were first made over the entire 4000–500 cm<sup>-1</sup> (2.5–20 μm) region using every fifth data point in the experimental spectrum (corresponding to ~1 point every 2.5 cm<sup>-1</sup>). The results of these calculations were then used to select appropriate  $n_0$  values for calculations from the same experimental spectra over the 2250–2050 cm<sup>-1</sup> region using all the available data points. The results of the higher resolution calculations were then adjusted to fit the continuous portions of the lower resolution results.

The absolute accuracy of the resulting optical constants is limited mainly by uncertainty in the assumed starting value of the visible refractive index ( $n_0$ ) of the ice sample and uncertainty in the measured sample thickness  $h$ . We have based our assumed  $n_0$  values on reported values for the visible refractive index of similar sample ices at the D lines of atomic Na ( $\lambda = 589$  nm). For ices dominated by CO<sub>2</sub>, N<sub>2</sub>, and O<sub>2</sub> we have used values of  $n_0 = 1.22$ , 1.22, and 1.25, respectively (Hallam & Scrimshaw 1973). We used a value of  $n_0 = 1.32$  for H<sub>2</sub>O-rich ices (Hudgins et al. 1993) and  $n_0 = 1.30$  for ices dominated by CO (Jiang, Person, & Brown 1975). In the cases of ices that were not clearly dominated by a single component, the concentration weighted values of the different ice components were used to estimate

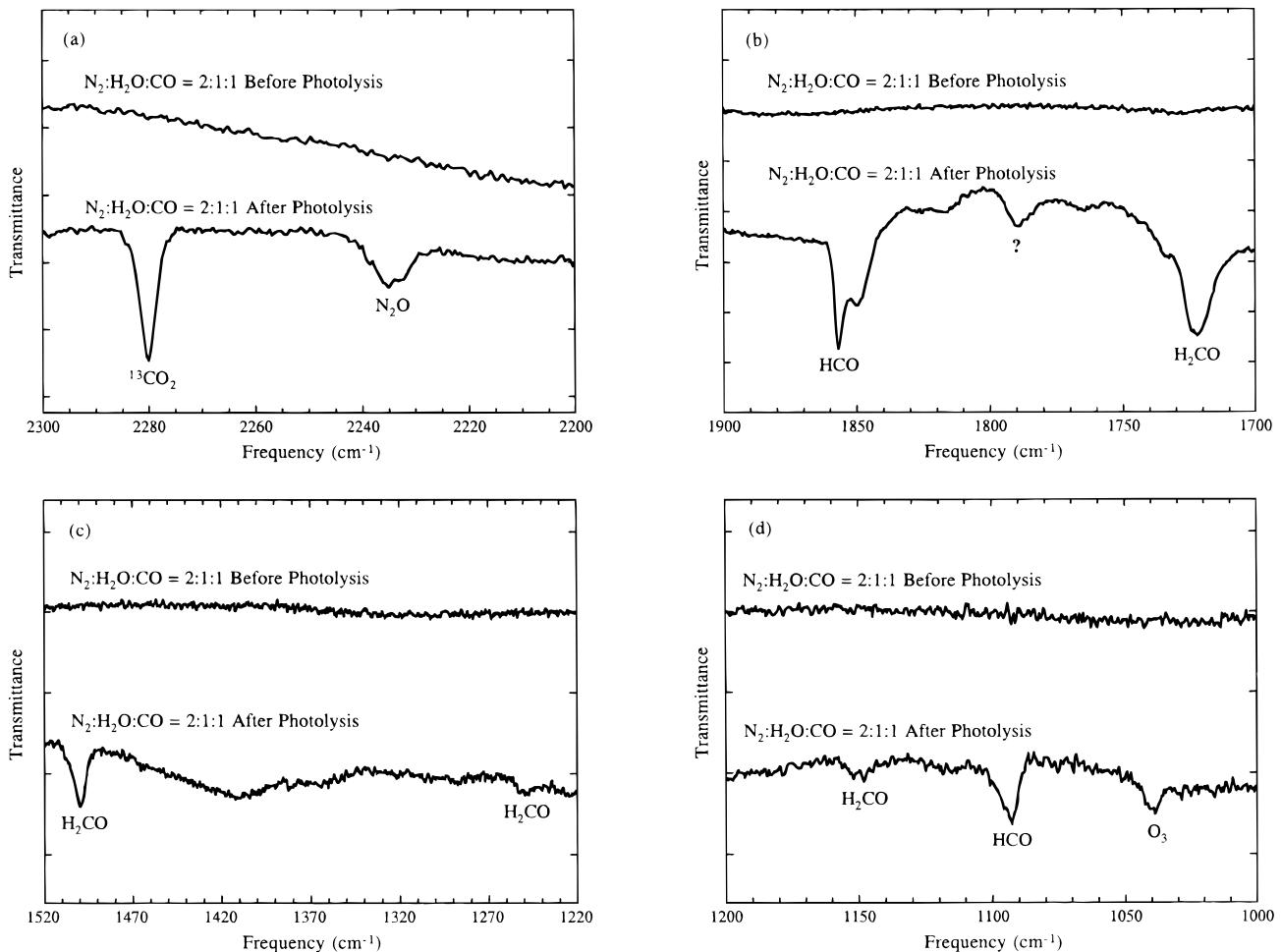


FIG. 8.—The new bands due to photoproducts made when an N<sub>2</sub>:H<sub>2</sub>O:CO = 2:1:1 ice at 12 K is UV irradiated for 3 hr. In all cases, the upper trace is of the ice prior to irradiation and the lower trace is of the ice after irradiation.

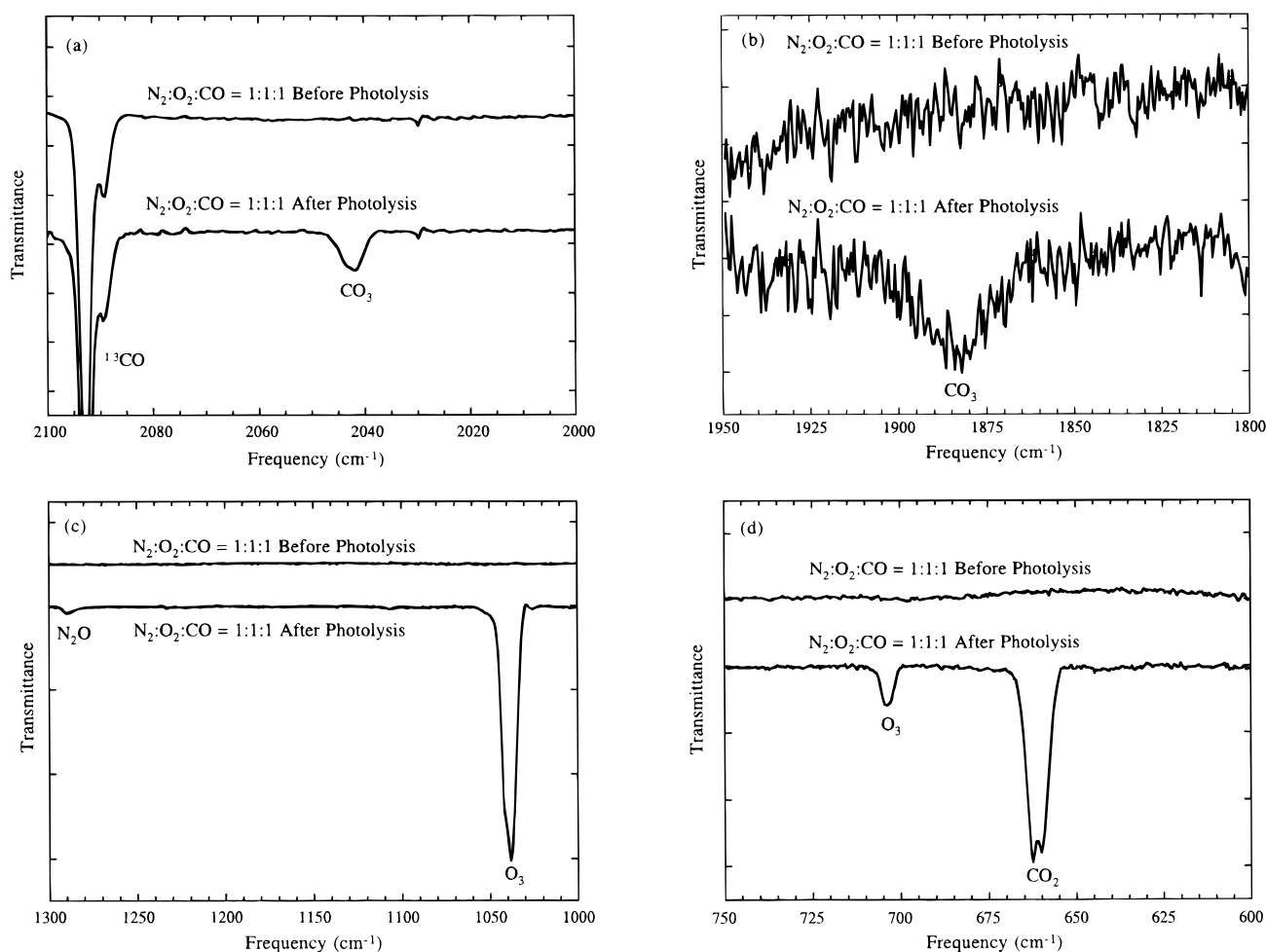


FIG. 9.—The new bands due to photoproducts made when an  $N_2:O_2:CO = 1:1:1$  ice at 12 K is UV irradiated for 3 hr. In all cases, the upper trace is of the ice prior to irradiation and the lower trace is of the ice after irradiation.

a value. Uncertainty in the adopted values for  $n_0$  is due to the effect of the residual dispersion of the ultraviolet contributions to  $n_0$  between the visible and  $4000\text{ cm}^{-1}$  and the dependence of  $n_0$  on the temperature, composition, and crystal structure of the sample. The effect of the above errors would largely be to impose a small global vertical shift on the resultant  $n$  values. Given the limited range of  $n_0$  values of these ices, we expect that the uncertainties associated with the values we have chosen are less than 5%.

The biggest difference between the techniques used by Hudgins et al. and those used here is that a laser was not used to determine sample thickness in this study. Here sample thicknesses were determined using two different methods. In many cases the samples were thick enough that a measurable portion of the infrared light underwent multiple reflections within the sample. This resulted in a sinusoidal interference pattern being superposed on the overall spectrum. In these cases the thickness of the ice could be determined from the equation

$$d = \frac{N_{\text{osc}}}{2n(\nu_0 - \nu_1)}, \quad (1)$$

where  $\nu_0$  and  $\nu_1$  are the limits (in  $\text{cm}^{-1}$ ) over which the oscillations due to interference are measured,  $N_{\text{osc}}$  is the number of fringes or “wavelengths” of the oscillation occurring between  $\nu_0$  and  $\nu_1$ , and  $n$  is the index of refraction

of the sample. In these cases, the accuracy of the thickness determination is largely limited by uncertainties in the value of  $n$ , uncertainties are probably less than 5%.

Absorption band strengths were used to estimate sample thicknesses in those cases for which the ice samples were too thin to produce measurable interference fringes. In this situation, the column density,  $N$  (in molecules  $\text{cm}^{-2}$ ), of different molecular species within the sample was determined using the equation

$$N_i = \frac{\int \tau_i(\nu) d\nu}{A_i}, \quad (2)$$

where  $\tau_i(\nu)$  is the frequency-dependent optical depth (in absorbance) of an absorption band and  $A_i$  is the band's integrated absorbance (in  $\text{cm molecule}^{-1}$ ) as determined from laboratory studies (see d'Hendecourt & Allamandola 1986; Hudgins et al. 1993). Column densities determined in this manner could be used with the known concentrations of the different molecules in the sample and a sample density based on matrix site sizes (Hallam & Scrimshaw 1973) to estimate a sample thickness. This technique is inherently less accurate than the interference technique because the actual densities and  $A_i$  values for these mixed molecular ices have not been measured and they can only be estimated from values obtained from similar, but less complex ices. When this technique was used on ice samples

TABLE 5

THE IDENTIFICATION OF FEATURES APPEARING UPON THE UV PHOTOLYSIS OF VARIOUS ICES CONTAINING N<sub>2</sub>, H<sub>2</sub>O, CO<sub>2</sub>, AND CO<sup>a</sup>

IDENTIFICATION	BAND POSITION (cm <sup>-1</sup> )							REFERENCE
	N <sub>2</sub> :CO 100:1	N <sub>2</sub> :CO 2:1	N <sub>2</sub> :CO 1:20	N <sub>2</sub> :H <sub>2</sub> O:CO 20:1:1	N <sub>2</sub> :H <sub>2</sub> O:CO 2:1:1	N <sub>2</sub> :O <sub>2</sub> :CO 1:1:1	N <sub>2</sub> :O <sub>2</sub> :CO <sub>2</sub> :CO 1:5:0.5:1	
CO <sub>2</sub> .....	<sup>b</sup>	3708.7 vw	3706.4 vw	<sup>c</sup>	<sup>c</sup>	3705.1 w	w <sup>d</sup>	Sandford & Allamandola 1990b
CO <sub>2</sub> .....	<sup>b</sup>	3603.2 vw	3601.7 vw	<sup>c</sup>	<sup>c</sup>	3600.9 w	w <sup>d</sup>	Sandford & Allamandola 1990b
CO <sub>2</sub> .....	2346.1 m	2347.3 m	2346.7 m	2348.8 s	2345.3 s	2347.0 s	vs <sup>d</sup>	Sandford & Allamandola 1990b
<sup>13</sup> CO <sub>2</sub> .....	...	2281.7 vw	2281.1 vw	2282.7 w	2279.2 w	2279.1 w	w <sup>d</sup>	Sandford & Allamandola 1990b
N <sub>2</sub> O.....	2234.7 m	2235.0 w	...	2235.6 w	2234.5 w	2234.1 w-m	2232.0 s	Dows 1957
O <sub>3</sub> .....	...	...	...	...	...	2108.0 w	2109.3 w	Bohn 1993
CO <sub>3</sub> .....	...	...	...	...	...	2041.4 w	2042.2 s	Moll et al. 1960
CO <sub>3</sub> .....	...	...	...	...	...	1881.1 vw	1888.4 w	Moll et al. 1960
HCO.....	...	...	...	1858.8 vw	1856.4 m	...	...	Milligan & Jacox 1971
?.....	...	...	...	...	1788.6 w	...	...	
H <sub>2</sub> CO.....	...	...	...	...	1721.3 m	...	...	Schutte et al. 1993
NO <sub>2</sub> , ?.....	1606.9 m	1604.0 vw	...	...	...	1607.4 vw	1607.9 w	St. Louis & Crawford 1965
H <sub>2</sub> CO.....	...	...	...	...	1499.3 w	...	...	Schutte et al. 1993
N <sub>2</sub> O.....	1290.7 w	1290.4 vw	...	1290.6 w	1287.0 vw	1289.8 w	1286.6 w	Dows 1957
H <sub>2</sub> CO.....	...	...	...	...	1247.2 vw	...	...	Schutte et al. 1993
?.....	...	...	...	...	...	...	1235 vw	
O <sub>3</sub> .....	...	...	...	...	...	1104.0 vw	...	Bohn 1993
H <sub>2</sub> CO.....	...	...	...	...	1147.6 vw	...	...	Schutte et al. 1993
HCO.....	...	...	...	...	1092.1 w	...	...	Milligan & Jacox 1971
O <sub>3</sub> .....	1040.8 m	1041.0 w	1038.6 w	1039.6 w	1037.7 w	1038.0 m	1037.0 vvs	Bohn 1993
CO <sub>3</sub> .....	...	...	...	...	...	975.0 vw	976 w	Dows 1957
O <sub>3</sub> .....	...	...	...	...	...	703.4 w	703.4 w	Bohn 1993
CO <sub>2</sub> .....	661.9 m	661.9 m	662.0 w	662.3 m	663.9 m	662.3 m	s <sup>d</sup>	Sandford & Allamandola 1990b

<sup>a</sup> vvs = very very strong, vs = very strong, s = strong, m = moderate, w = weak, vw = very weak, vvw = very, very weak with respect to the very strong CO absorption after 3 hr of photolysis.

<sup>b</sup> Weak absorptions obscured by bands due to minor contaminant H<sub>2</sub>O.

<sup>c</sup> Obscured by H<sub>2</sub>O bands.

<sup>d</sup> Total CO<sub>2</sub> band areas increase by a factor of ~2 upon photolysis, implying CO<sub>2</sub> production.

for which we had independent thickness determinations from interference measurements, it was found that thicknesses based on absorption band strengths fell within 50% of the values determined from fringe analysis.

A summary of the  $n$  and  $k$  values of the CO feature in a number of ices are listed in Tables 7 and 8. The values we assumed for  $n_{(\text{NaD})}$  and  $d$  for each sample are also in the tables. It can be seen that the majority of our sample thicknesses fell within the 0.1–5.0  $\mu\text{m}$  range, although ices dominated by strong absorbers like CO<sub>2</sub> were occasionally thinner and ices dominated by weak absorbers such as N<sub>2</sub> and O<sub>2</sub> were occasionally thicker. The expected absolute accuracies of these values differ from ice to ice and depend largely on uncertainties in the sample thicknesses. For ices whose thicknesses were determined from interference fringes produced by internal reflections (N<sub>2</sub>:CO = 2:1, O<sub>2</sub>:CO = 20:1, N<sub>2</sub>:H<sub>2</sub>O:CO = 2:1:1), we estimate the *absolute* uncertainty of the calculated optical constants to be about 5%. Uncertainties differ for ices where the thick-

ness could only be estimated from absorption band strengths. For the pure CO ice and the ices H<sub>2</sub>O:CO = 20:1 and CO<sub>2</sub>:CO = 20:1, where  $A$ -values have been measured for similar ices, absolute uncertainties are probably less than 10%. The uncertainties associated with the other ices listed in Tables 7 and 8 (N<sub>2</sub>:O<sub>2</sub>:CO<sub>2</sub>:CO = 1:5: $\frac{1}{2}$ :1, N<sub>2</sub>:CO<sub>2</sub>:CO = 1:5:1, N<sub>2</sub>:H<sub>2</sub>O:CO = 5:1:5, N<sub>2</sub>:O<sub>2</sub>:CO = 1:5:1) are likely to be similar, but could be as large as 50%. We stress, however, that the *relative* errors between adjacent  $n$  and  $k$  pairs in all the columns are less than 0.1%, the limiting difference between the measured and calculated spectra at which we chose to terminate our iterative calculations.

#### 3.4. The Fundamental Bands of Solid N<sub>2</sub> and O<sub>2</sub>

Although neither N<sub>2</sub> nor O<sub>2</sub> have allowed infrared transitions, it has long been known that infrared activity is induced when these species are condensed (Smith, Keller, & Johnston 1950). Use of this effect has been proposed by

TABLE 6

CO PEAK POSITION AND FWHM AT 12 K BEFORE AND AFTER UV PHOTOLYSIS

Ice Composition	Prephotolysis CO Position (FWHM) (cm <sup>-1</sup> )	Postphotolysis CO Position (FWHM) (cm <sup>-1</sup> )
N <sub>2</sub> :CO = 100:1 .....	2139.6 (1.1)	2139.6 (1.1)
N <sub>2</sub> :CO = 2:1 .....	2138.7 (2.6)	2139.2 (3.0)
N <sub>2</sub> :CO = 1:20 .....	2138.2 (2.6)	2139.7 (2.6)
N <sub>2</sub> :H <sub>2</sub> O:CO = 19:1:1 .....	2139.6 (1.6)	2139.6 (1.6)
N <sub>2</sub> :H <sub>2</sub> O:CO = 2:1:1 .....	2139.2 (5.3)	2139.2 (5.3)
N <sub>2</sub> :O <sub>2</sub> :CO = 1:1:1 .....	2139.2 (4.0)	2139.2 (6.0)
N <sub>2</sub> :O <sub>2</sub> :CO <sub>2</sub> :CO = 1:5:0.5:1 .....	2141.0 (7.1)	2141.1 (7.7)

TABLE 7  
OPTICAL CONSTANTS

FREQUENCY ( $\text{cm}^{-1}$ )	$\text{N}_2:\text{O}_2:\text{CO}_2:\text{CO}$ = 1:5:0.5:1 ( $n_0 = 1.24$ ) ( $d = 1.85 \times 10^{-5}$ cm)		$\text{H}_2\text{O}:\text{CO}$ = 20:1 ( $n_0 = 1.32$ ) ( $d = 4.35 \times 10^{-5}$ cm)		$\text{N}_2:\text{CO}_2:\text{CO}$ = 1:5:1 ( $n = 1.22$ ) ( $d = 6.5 \times 10^{-6}$ cm)		$\text{N}_2:\text{H}_2\text{O}:\text{CO}$ = 5:1:5 ( $n_0 = 1.27$ ) ( $d = 2.56 \times 10^{-5}$ cm)		$\text{N}_2:\text{O}_2:\text{CO}$ = 1:5:1 ( $n_0 = 1.25$ ) ( $d = 8.1 \times 10^{-5}$ cm)	
	$n$	$k$	$n$	$k$	$n$	$k$	$n$	$k$	$n$	$k$
2065.4.....	1.2550	0.0003	1.3512	0.0065	1.2917	0.0001	1.2852	0.0009	1.2578	0.0005
2073.1.....	1.2561	0.0007	1.3521	0.0070	1.2931	0.0001	1.2872	0.0009	1.2585	0.0005
2080.9.....	1.2569	0.0007	1.3531	0.0077	1.2962	0.0006	1.2904	0.0012	1.2599	0.0006
2088.6.....	1.2585	0.0017	1.3540	0.0087	1.2997	0.0003	1.2964	0.0037	1.2622	0.0019
2096.3.....	1.2576	0.0029	1.3547	0.0088	1.3019	0.0027	1.2919	0.0014	1.2607	0.0009
2098.7.....	1.2581	0.0020	1.3553	0.0089	1.3013	0.0024	1.2952	0.0015	1.2618	0.0008
2101.1.....	1.2588	0.0019	1.3556	0.0091	1.3043	0.0002	1.2974	0.0011	1.2630	0.0008
2103.5.....	1.2594	0.0014	1.3563	0.0090	1.3061	0.0000	1.2999	0.0006	1.2639	0.0007
2105.9.....	1.2604	0.0018	1.3567	0.0095	1.3075	0.0009	1.3023	0.0008	1.2649	0.0009
2108.3.....	1.2615	0.0011	1.3575	0.0094	1.3101	0.0007	1.3057	0.0003	1.2662	0.0007
2110.8.....	1.2626	0.0013	1.3582	0.0097	1.3114	0.0002	1.3088	0.0007	1.2677	0.0008
2113.2.....	1.2637	0.0016	1.3589	0.0098	1.3138	0.0010	1.3127	0.0010	1.2693	0.0009
2115.6.....	1.2651	0.0016	1.3600	0.0099	1.3153	0.0015	1.3167	0.0000	1.2712	0.0007
2116.5.....	1.2658	0.0014	1.3604	0.0101	1.3171	0.0017	1.3189	0.0000	1.2721	0.0006
2117.5.....	1.2666	0.0012	1.3609	0.0100	1.3176	0.0018	1.3213	0.0000	1.2732	0.0007
2118.5.....	1.2675	0.0010	1.3614	0.0102	1.3186	0.0015	1.3239	0.0000	1.2743	0.0007
2119.4.....	1.2682	0.0011	1.3621	0.0102	1.3186	0.0007	1.3264	0.0001	1.2753	0.0007
2120.4.....	1.2696	0.0002	1.3628	0.0104	1.3222	0.0000	1.3293	0.0000	1.2768	0.0007
2121.4.....	1.2707	0.0014	1.3636	0.0104	1.3234	0.0005	1.3326	0.0000	1.2783	0.0008
2122.3.....	1.2716	0.0010	1.3646	0.0105	1.3253	0.0013	1.3358	0.0000	1.2798	0.0008
2123.3.....	1.2731	0.0011	1.3657	0.0107	1.3259	0.0014	1.3397	0.0000	1.2816	0.0008
2124.3.....	1.2747	0.0002	1.3670	0.0107	1.3279	0.0000	1.3443	0.0000	1.2838	0.0006
2125.2.....	1.2764	0.0010	1.3685	0.0109	1.3311	0.0004	1.3491	0.0000	1.2862	0.0005
2126.2.....	1.2782	0.0005	1.3707	0.0113	1.3341	0.0020	1.3549	0.0000	1.2891	0.0008
2127.2.....	1.2804	0.0008	1.3734	0.0120	1.3344	0.0038	1.3614	0.0000	1.2924	0.0008
2128.1.....	1.2832	0.0000	1.3760	0.0134	1.3371	0.0000	1.3686	0.0000	1.2960	0.0006
2129.1.....	1.2864	0.0005	1.3797	0.0158	1.3419	0.0024	1.3781	0.0000	1.3009	0.0006
2130.0.....	1.2895	0.0006	1.3834	0.0197	1.3449	0.0018	1.3882	0.0000	1.3063	0.0005
2130.5.....	1.2919	0.0000	1.3860	0.0223	1.3475	0.0028	1.3942	0.0000	1.3099	0.0006
2131.0.....	1.2947	0.0001	1.3861	0.0255	1.3494	0.0043	1.4013	0.0000	1.3139	0.0005
2131.5.....	1.2975	0.0008	1.3878	0.0293	1.3516	0.0036	1.4094	0.0000	1.3186	0.0004
2132.0.....	1.3005	0.0007	1.3884	0.0336	1.3554	0.0028	1.4186	0.0000	1.3242	0.0002
2132.5.....	1.3041	0.0012	1.3883	0.0385	1.3586	0.0047	1.4289	0.0000	1.3309	0.0002
2132.9.....	1.3073	0.0009	1.3877	0.0434	1.3624	0.0088	1.4387	0.0000	1.3373	0.0001
2133.4.....	1.3123	0.0014	1.3865	0.0486	1.3658	0.0110	1.4518	0.0000	1.3472	0.0002
2133.9.....	1.3183	0.0017	1.3838	0.0535	1.3692	0.0137	1.4676	0.0000	1.3601	0.0006
2134.4.....	1.3256	0.0033	1.3802	0.0580	1.3729	0.0170	1.4866	0.0000	1.3772	0.0028
2134.9.....	1.3346	0.0054	1.3760	0.0621	1.3767	0.0215	1.5098	0.0002	1.3996	0.0098
2135.4.....	1.3469	0.0104	1.3708	0.0656	1.3828	0.0269	1.5390	0.0038	1.4308	0.0273
2135.8.....	1.3538	0.0190	1.3674	0.0680	1.3831	0.0319	1.5648	0.0110	1.4425	0.0632
2136.3.....	1.3653	0.0337	1.3592	0.0695	1.3870	0.0385	1.6049	0.0232	1.4565	0.1159
2136.8.....	1.3724	0.0535	1.3553	0.0697	1.3893	0.0485	1.6529	0.0424	1.4485	0.1737
2137.3.....	1.3742	0.0781	1.3492	0.0691	1.3901	0.0579	1.7136	0.0702	1.4252	0.2229
2137.8.....	1.3707	0.1027	1.3434	0.0672	1.3913	0.0683	1.8143	0.1096	1.4018	0.2603
2138.2.....	1.3578	0.1261	1.3399	0.0644	1.3874	0.0787	1.8704	0.2121	1.3452	0.3011
2138.7.....	1.3440	0.1436	1.3343	0.0610	1.3857	0.0892	1.9520	0.4344	1.3172	0.3422
2139.2.....	1.3288	0.1568	1.3326	0.0574	1.3806	0.0985	1.8910	0.7995	1.2451	0.3700
2139.7.....	1.3105	0.1658	1.3299	0.0533	1.3751	0.1078	1.6565	1.0962	1.1648	0.3622
2140.2.....	1.2922	0.1714	1.3281	0.0493	1.3680	0.1174	1.3327	1.1738	1.0922	0.3164
2140.7.....	1.2726	0.1754	1.3268	0.0455	1.3637	0.1264	1.1560	1.0445	1.0605	0.2488
2141.1.....	1.2500	0.1826	1.3263	0.0419	1.3490	0.1345	0.8035	0.9670	1.0302	0.1729
2141.6.....	1.2370	0.1846	1.3264	0.0383	1.3411	0.1398	0.7135	0.7309	1.0310	0.1076
2142.1.....	1.2192	0.1844	1.3272	0.0353	1.3287	0.1427	0.6552	0.4467	1.0495	0.0545
2142.6.....	1.1956	0.1795	1.3279	0.0327	1.3163	0.1451	0.7025	0.2270	1.0771	0.0209
2143.1.....	1.1721	0.1677	1.3289	0.0304	1.3027	0.1454	0.7870	0.1240	1.1046	0.0061
2143.6.....	1.1566	0.1492	1.3299	0.0286	1.2978	0.1418	0.8676	0.0717	1.1266	0.0013
2144.0.....	1.1411	0.1277	1.3316	0.0271	1.2753	0.1384	0.9104	0.0441	1.1402	0.0000
2144.5.....	1.1350	0.1033	1.3319	0.0260	1.2713	0.1299	0.9690	0.0338	1.1534	0.0000
2145.0.....	1.1325	0.0805	1.3336	0.0252	1.2619	0.1222	1.0090	0.0305	1.1635	0.0000
2145.5.....	1.1345	0.0598	1.3347	0.0246	1.2535	0.1136	1.0393	0.0317	1.1714	0.0002
2146.0.....	1.1433	0.0428	1.3357	0.0243	1.2497	0.1046	1.0644	0.0368	1.1780	0.0004
2146.4.....	1.1488	0.0301	1.3371	0.0242	1.2419	0.0939	1.0692	0.0406	1.1824	0.0003
2146.9.....	1.1562	0.0211	1.3370	0.0241	1.2396	0.0838	1.0818	0.0414	1.1872	0.0006
2147.4.....	1.1647	0.0144	1.3381	0.0243	1.2369	0.0722	1.0888	0.0371	1.1913	0.0007
2147.9.....	1.1724	0.0105	1.3386	0.0246	1.2370	0.0603	1.0964	0.0307	1.1949	0.0008
2148.4.....	1.1790	0.0076	1.3389	0.0248	1.2377	0.0526	1.1050	0.0241	1.1980	0.0009
2148.9.....	1.1851	0.0059	1.3390	0.0250	1.2393	0.0432	1.1159	0.0197	1.2009	0.0010

TABLE 7—Continued

FREQUENCY (cm <sup>-1</sup> )	N <sub>2</sub> :O <sub>2</sub> :CO <sub>2</sub> :CO = 1:5:0.5:1 (n <sub>0</sub> = 1.24) (d = 1.85 × 10 <sup>-5</sup> cm)		H <sub>2</sub> O:CO = 20:1 (n <sub>0</sub> = 1.32) (d = 4.35 × 10 <sup>-5</sup> cm)		N <sub>2</sub> :CO <sub>2</sub> :CO = 1:5:1 (n = 1.22) (d = 6.5 × 10 <sup>-6</sup> cm)		N <sub>2</sub> :H <sub>2</sub> O:CO = 5:1:5 (n <sub>0</sub> = 1.27) (d = 2.56 × 10 <sup>-5</sup> cm)		N <sub>2</sub> :O <sub>2</sub> :CO = 1:5:1 (n <sub>0</sub> = 1.25) (d = 8.1 × 10 <sup>-5</sup> cm)	
	n	k	n	k	n	k	n	k	n	k
2149.3.....	1.1885	0.0041	1.3392	0.0253	1.2401	0.0365	1.1202	0.0165	1.2028	0.0010
2149.8.....	1.1936	0.0035	1.3392	0.0253	1.2441	0.0299	1.1303	0.0151	1.2052	0.0010
2150.3.....	1.1975	0.0031	1.3393	0.0255	1.2472	0.0228	1.1373	0.0140	1.2073	0.0010
2150.8.....	1.2006	0.0028	1.3391	0.0257	1.2511	0.0170	1.1433	0.0129	1.2092	0.0010
2151.3.....	1.2037	0.0019	1.3389	0.0260	1.2565	0.0120	1.1498	0.0114	1.2111	0.0010
2151.7.....	1.2058	0.0018	1.3388	0.0262	1.2586	0.0094	1.1523	0.0102	1.2122	0.0010
2152.2.....	1.2083	0.0020	1.3380	0.0262	1.2637	0.0075	1.1581	0.0098	1.2138	0.0011
2152.7.....	1.2101	0.0020	1.3378	0.0262	1.2675	0.0057	1.1623	0.0087	1.2152	0.0012
2153.2.....	1.2120	0.0011	1.3372	0.0261	1.2707	0.0051	1.1665	0.0075	1.2165	0.0012
2153.7.....	1.2140	0.0009	1.3366	0.0257	1.2735	0.0035	1.1703	0.0070	1.2176	0.0013
2154.2.....	1.2156	0.0014	1.3361	0.0252	1.2765	0.0023	1.1743	0.0059	1.2188	0.0012
2154.6.....	1.2166	0.0007	1.3359	0.0248	1.2786	0.0010	1.1763	0.0048	1.2195	0.0011
2155.1.....	1.2183	0.0008	1.3354	0.0242	1.2818	0.0009	1.1806	0.0038	1.2206	0.0012
2156.1.....	1.2209	0.0008	1.3350	0.0230	1.2861	0.0010	1.1870	0.0037	1.2224	0.0013
2157.1.....	1.2231	0.0009	1.3347	0.0216	1.2900	0.0015	1.1928	0.0033	1.2242	0.0013
2158.0.....	1.2246	0.0009	1.3346	0.0201	1.2915	0.0012	1.1968	0.0030	1.2253	0.0014
2159.0.....	1.2261	0.0007	1.3352	0.0187	1.2959	0.0000	1.2012	0.0026	1.2266	0.0013
2159.9.....	1.2275	0.0003	1.3357	0.0177	1.2985	0.0019	1.2044	0.0029	1.2275	0.0015
2160.9.....	1.2291	0.0001	1.3364	0.0165	1.2996	0.0000	1.2083	0.0025	1.2287	0.0016
2161.9.....	1.2303	0.0006	1.3373	0.0158	1.3019	0.0005	1.2112	0.0028	1.2296	0.0016
2162.8.....	1.2312	0.0004	1.3383	0.0152	1.3050	0.0000	1.2140	0.0024	1.2303	0.0016
2163.8.....	1.2322	0.0002	1.3390	0.0150	1.3063	0.0008	1.2165	0.0033	1.2312	0.0017
2164.8.....	1.2333	0.0002	1.3397	0.0148	1.3074	0.0010	1.2186	0.0030	1.2319	0.0018
2165.7.....	1.2340	0.0004	1.3403	0.0145	1.3083	0.0000	1.2203	0.0028	1.2323	0.0016
2166.7.....	1.2352	0.0000	1.3410	0.0147	1.3113	0.0009	1.2229	0.0030	1.2333	0.0018
2167.7.....	1.2357	0.0005	1.3414	0.0148	1.3124	0.0008	1.2248	0.0033	1.2339	0.0019
2168.6.....	1.2362	0.0002	1.3418	0.0146	1.3127	0.0021	1.2261	0.0034	1.2342	0.0018
2169.6.....	1.2371	0.0000	1.3423	0.0147	1.3140	0.0000	1.2276	0.0027	1.2348	0.0017
2172.0.....	1.2385	0.0000	1.3428	0.0147	1.3177	0.0007	1.2309	0.0037	1.2358	0.0019
2174.4.....	1.2397	0.0004	1.3433	0.0149	1.3221	0.0000	1.2341	0.0040	1.2367	0.0020
2176.8.....	1.2408	0.0000	1.3437	0.0149	1.3232	0.0000	1.2361	0.0037	1.2375	0.0019
2179.2.....	1.2420	0.0001	1.3440	0.0152	1.3254	0.0018	1.2378	0.0046	1.2379	0.0022
2181.6.....	1.2431	0.0000	1.3441	0.0152	1.3300	0.0008	1.2392	0.0048	1.2385	0.0021
2184.1.....	1.2442	0.0000	1.3443	0.0155	1.3326	0.0008	1.2417	0.0039	1.2394	0.0019
2186.5.....	1.2447	0.0000	1.3443	0.0153	1.3331	0.0021	1.2423	0.0043	1.2395	0.0020
2188.9.....	1.2460	0.0000	1.3445	0.0156	1.3360	0.0012	1.2438	0.0048	1.2400	0.0020
2191.3.....	1.2467	0.0000	1.3446	0.0152	1.3396	0.0008	1.2450	0.0048	1.2404	0.0020
2193.7.....	1.2475	0.0000	1.3449	0.0156	1.3412	0.0000	1.2458	0.0045	1.2407	0.0019
2196.1.....	1.2480	0.0000	1.3447	0.0155	1.3440	0.0000	1.2464	0.0051	1.2409	0.0020
2204.3.....	1.2506	0.0000	1.3449	0.0154	1.3525	0.0018	1.2486	0.0045	1.2417	0.0017
2211.5.....	1.2525	0.0000	1.3448	0.0152	1.3592	0.0002	1.2493	0.0045	1.2422	0.0015
2219.7.....	1.2545	0.0000	1.3446	0.0151	1.3692	0.0000	1.2497	0.0034	1.2425	0.0013
2227.9.....	1.2562	0.0002	1.3448	0.0148	1.3778	0.0004	1.2514	0.0009	1.2430	0.0009

Ehrenfreund et al. (1992) to search for frozen, interstellar O<sub>2</sub>, and was exploited by Sandford, Allamandola, & Geballe (1993) to detect frozen interstellar H<sub>2</sub>. The overtone of the solid N<sub>2</sub> feature at 4651 cm<sup>-1</sup> (2.15 μm) has been detected in Triton and Pluto (Cruikshank et al. 1993; Owen et al. 1993).

The N<sub>2</sub> band falls at 2327.7 cm<sup>-1</sup> (4.2961 μm) (Fig. 10) in a spectral region obscured by telluric CO<sub>2</sub>. The 2327.7 cm<sup>-1</sup> band has been well studied and is readily attributable to N<sub>2</sub> (Moll, Clutter, & Thompson 1960; Löwen, Bier, & Jodl 1990; Grundy, Schmitt, & Quirico 1993; Bohn et al. 1994; Tryka, Brown, & Anicich 1995). As discussed by Ehrenfreund et al. (1992), O<sub>2</sub> frozen in mixed-molecular ices also has weak infrared activity. Figure 11 shows the O<sub>2</sub> band in a N<sub>2</sub>:O<sub>2</sub>:CO = 1:1:1 ice before and after 3 hr of UV irradiation. The feature falls near 1549 cm<sup>-1</sup> (6.456 μm).

4. THE INTERSTELLAR CO BAND AND NONPOLAR ICES

The previous results will now be discussed in an astro-

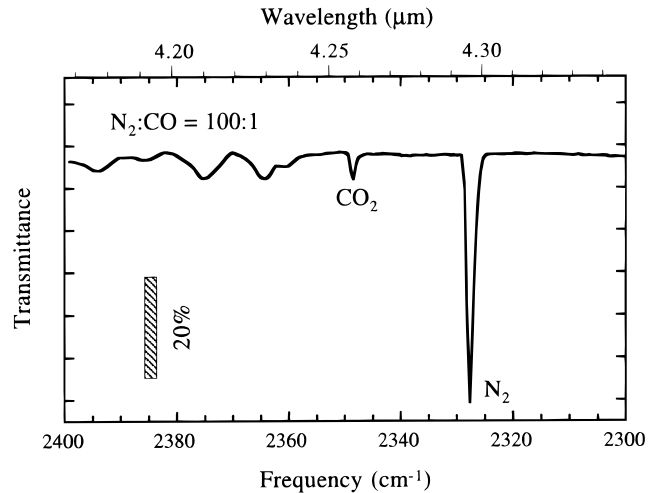


FIG. 10.—The N<sub>2</sub> stretching bands produced by an N<sub>2</sub>:CO = 1:100 ice at 12 K.

TABLE 8  
OPTICAL CONSTANTS

FREQUENCY (cm <sup>-1</sup> )	Pure CO ( $n_0 = 1.30$ ) ( $d = 8.0 \times 10^{-6}$ cm)		N <sub>2</sub> :CO = 2:1 ( $n_0 = 1.25$ ) ( $d = 5.87 \times 10^{-5}$ cm)		O <sub>2</sub> :CO = 20:1 ( $n_0 = 1.25$ ) ( $d = 1.15 \times 10^{-4}$ cm)		CO <sub>2</sub> :CO = 20:1 ( $n_0 = 1.22$ ) ( $d = 1.65 \times 10^{-6}$ cm)		N <sub>2</sub> :H <sub>2</sub> O:CO = 2:1:1 ( $n_0 = 1.27$ ) ( $d = 1.0 \times 10^{-4}$ cm)	
	<i>n</i>	<i>k</i>	<i>n</i>	<i>k</i>	<i>n</i>	<i>k</i>	<i>n</i>	<i>k</i>	<i>n</i>	<i>k</i>
2057.7.....	1.3371	0.0010	1.2571	0.0007	1.2529	0.0000	1.3035	0.0000	1.2799	0.0001
2065.5.....	1.3395	0.0017	1.2577	0.0007	1.2532	0.0000	1.3051	0.0001	1.2808	0.0001
2073.2.....	1.3457	0.0030	1.2585	0.0007	1.2536	0.0000	1.3059	0.0001	1.2819	0.0003
2080.9.....	1.3538	0.0030	1.2597	0.0009	1.2542	0.0000	1.3074	0.0003	1.2836	0.0002
2088.6.....	1.3614	0.0111	1.2623	0.0023	1.2558	0.0008	1.3097	0.0000	1.2862	0.0014
2096.3.....	1.3525	0.0038	1.2604	0.0009	1.2549	0.0000	1.3118	0.0000	1.2858	0.0010
2098.7.....	1.3594	0.0025	1.2616	0.0009	1.2554	0.0000	1.3126	0.0000	1.2872	0.0011
2101.1.....	1.3651	0.0035	1.2628	0.0008	1.2558	0.0000	1.3136	0.0000	1.2879	0.0015
2103.6.....	1.3710	0.0028	1.2638	0.0008	1.2563	0.0000	1.3144	0.0000	1.2887	0.0011
2106.0.....	1.3766	0.0024	1.2649	0.0012	1.2568	0.0000	1.3153	0.0000	1.2899	0.0004
2108.4.....	1.3829	0.0019	1.2660	0.0010	1.2574	0.0000	1.3163	0.0000	1.2916	0.0002
2110.8.....	1.3883	0.0023	1.2673	0.0013	1.2580	0.0001	1.3174	0.0002	1.2937	0.0002
2113.2.....	1.3956	0.0024	1.2690	0.0017	1.2588	0.0001	1.3185	0.0005	1.2958	0.0003
2115.6.....	1.4061	0.0015	1.2706	0.0016	1.2598	0.0000	1.3194	0.0010	1.2983	0.0002
2116.6.....	1.4105	0.0008	1.2716	0.0014	1.2603	0.0000	1.3197	0.0003	1.2993	0.0002
2117.5.....	1.4154	0.0003	1.2725	0.0017	1.2608	0.0000	1.3205	0.0000	1.3006	0.0001
2118.5.....	1.4210	0.0000	1.2735	0.0017	1.2614	0.0000	1.3214	0.0005	1.3020	0.0002
2119.5.....	1.4289	0.0000	1.2745	0.0019	1.2620	0.0000	1.3216	0.0007	1.3033	0.0002
2120.4.....	1.4346	0.0017	1.2758	0.0017	1.2627	0.0000	1.3221	0.0004	1.3050	0.0002
2121.4.....	1.4404	0.0008	1.2772	0.0020	1.2635	0.0000	1.3228	0.0005	1.3067	0.0002
2122.4.....	1.4491	0.0000	1.2786	0.0020	1.2643	0.0000	1.3234	0.0003	1.3085	0.0002
2123.3.....	1.4582	0.0000	1.2802	0.0022	1.2653	0.0000	1.3243	0.0002	1.3108	0.0003
2124.3.....	1.4687	0.0002	1.2821	0.0020	1.2666	0.0000	1.3252	0.0002	1.3132	0.0002
2125.2.....	1.4795	0.0000	1.2843	0.0025	1.2677	0.0000	1.3261	0.0002	1.3158	0.0001
2126.2.....	1.4921	0.0005	1.2864	0.0026	1.2694	0.0000	1.3271	0.0002	1.3191	0.0002
2127.2.....	1.5080	0.0000	1.2894	0.0025	1.2713	0.0001	1.3284	0.0004	1.3229	0.0002
2128.1.....	1.5263	0.0000	1.2926	0.0026	1.2734	0.0000	1.3295	0.0003	1.3269	0.0002
2129.1.....	1.5485	0.0000	1.2965	0.0029	1.2763	0.0001	1.3311	0.0007	1.3323	0.0003
2130.1.....	1.5757	0.0000	1.3013	0.0031	1.2796	0.0002	1.3226	0.0009	1.3381	0.0004
2130.6.....	1.5929	0.0000	1.3040	0.0031	1.2818	0.0003	1.3337	0.0009	1.3420	0.0004
2131.0.....	1.6093	0.0000	1.3071	0.0034	1.2845	0.0002	1.3344	0.0011	1.3464	0.0007
2131.5.....	1.6308	0.0000	1.3106	0.0034	1.2877	0.0004	1.3356	0.0015	1.3513	0.0010
2132.0.....	1.6558	0.0000	1.3145	0.0035	1.2915	0.0004	1.3367	0.0020	1.3571	0.0014
2132.5.....	1.6848	0.0000	1.3191	0.0037	1.2963	0.0006	1.3379	0.0024	1.3642	0.0020
2133.0.....	1.7197	0.0013	1.3244	0.0040	1.3009	0.0007	1.3394	0.0030	1.3700	0.0032
2133.4.....	1.7527	0.0046	1.3306	0.0042	1.3087	0.0012	1.3399	0.0035	1.3793	0.0052
2133.9.....	1.8025	0.0145	1.3384	0.0049	1.3195	0.0022	1.3417	0.0041	1.3898	0.0085
2134.4.....	1.8597	0.0354	1.3475	0.0056	1.3348	0.0059	1.3434	0.0051	1.4021	0.0135
2134.9.....	1.9218	0.0702	1.3588	0.0072	1.3564	0.0165	1.3451	0.0063	1.4163	0.0216
2135.4.....	1.9869	0.1153	1.3727	0.0103	1.3887	0.0474	1.3470	0.0078	1.4344	0.0337
2135.9.....	2.0850	0.1559	1.3900	0.0164	1.3788	0.1197	1.3497	0.0096	1.4419	0.0523
2136.3.....	2.1355	0.2202	1.4099	0.0254	1.3359	0.2133	1.3505	0.0125	1.4586	0.0780
2136.8.....	2.2776	0.3211	1.4351	0.0376	1.2594	0.2077	1.3525	0.0156	1.4669	0.1126
2137.3.....	2.4159	0.5410	1.4705	0.0549	1.2300	0.1492	1.3539	0.0194	1.4670	0.1552
2137.8.....	2.4569	0.9843	1.5190	0.0951	1.2143	0.1276	1.3549	0.0243	1.4626	0.2015
2138.3.....	2.4082	1.4714	1.5643	0.2098	1.2000	0.1168	1.3558	0.0291	1.4253	0.2489
2138.7.....	1.8141	2.0591	1.5250	0.4303	1.1882	0.1057	1.3541	0.0385	1.4018	0.2893
2139.2.....	1.3942	1.9681	1.3614	0.6073	1.1771	0.0889	1.3503	0.0453	1.3492	0.3251
2139.7.....	0.9789	1.7307	1.1538	0.5721	1.1708	0.0694	1.3435	0.0510	1.2836	0.3435
2140.2.....	0.8075	1.4179	1.0286	0.4149	1.1694	0.0500	1.3359	0.0529	1.2140	0.3263
2140.7.....	0.7100	1.1613	0.9820	0.2683	1.1745	0.0348	1.3286	0.0521	1.1812	0.2804
2141.2.....	0.6186	0.8724	0.9872	0.1690	1.1785	0.0219	1.3254	0.0464	1.1287	0.2226
2141.6.....	0.5781	0.5796	1.0087	0.1061	1.1842	0.0122	1.3200	0.0497	1.1267	0.1680
2142.1.....	0.5384	0.6529	1.0328	0.0635	1.1919	0.0060	1.3179	0.0455	1.1307	0.1224
2142.6.....	0.5228	0.5934	1.0597	0.0306	1.1988	0.0027	1.3149	0.0436	1.1438	0.0891
2143.1.....	0.5391	0.4825	1.0868	0.0085	1.2048	0.0008	1.3121	0.0417	1.1608	0.0664
2143.6.....	0.5635	0.3066	1.1116	0.0016	1.2096	0.0000	1.3089	0.0398	1.1814	0.0532
2144.1.....	0.6203	0.1642	1.1302	0.0000	1.2130	0.0000	1.3072	0.0342	1.1915	0.0464
2144.5.....	0.6681	0.1050	1.1443	0.0000	1.2163	0.0000	1.3061	0.0352	1.2099	0.0458
2145.0.....	0.7553	0.0725	1.1552	0.0000	1.2191	0.0000	1.3055	0.0314	1.2225	0.0486
2145.5.....	0.8156	0.0536	1.1641	0.0000	1.2214	0.0000	1.3047	0.0290	1.2321	0.0542
2146.0.....	0.8642	0.0457	1.1714	0.0000	1.2233	0.0000	1.3038	0.0271	1.2397	0.0619
2146.5.....	0.9056	0.0426	1.1775	0.0000	1.2247	0.0000	1.3037	0.0237	1.2413	0.0703
2146.9.....	0.9224	0.0405	1.1827	0.0000	1.2262	0.0000	1.3037	0.0232	1.2421	0.0794
2147.4.....	0.9512	0.0350	1.1871	0.0000	1.2276	0.0000	1.3036	0.0203	1.2385	0.0877
2147.9.....	0.9740	0.0294	1.1909	0.0000	1.2287	0.0000	1.3039	0.0187	1.2325	0.0947
2148.4.....	1.0148	0.0259	1.1944	0.0000	1.2298	0.0000	1.3041	0.0173	1.2238	0.0993

TABLE 8—Continued

FREQUENCY (cm <sup>-1</sup> )	Pure CO (n <sub>0</sub> = 1.30) (d = 8.0 × 10 <sup>-6</sup> cm)		N <sub>2</sub> :CO = 2:1 (n <sub>0</sub> = 1.25) (d = 5.87 × 10 <sup>-5</sup> cm)		O <sub>2</sub> :CO = 20:1 (n <sub>0</sub> = 1.25) (d = 1.15 × 10 <sup>-4</sup> cm)		CO <sub>2</sub> :CO = 20:1 (n <sub>0</sub> = 1.22) (d = 1.65 × 10 <sup>-6</sup> cm)		N <sub>2</sub> :H <sub>2</sub> O:CO = 2:1:1 (n <sub>0</sub> = 1.27) (d = 1.0 × 10 <sup>-4</sup> cm)	
	n	k	n	k	n	k	n	k	n	k
2148.9.....	1.0133	0.0232	1.1975	0.0000	1.2307	0.0000	1.3041	0.0158	1.2169	0.1014
2149.4.....	1.0315	0.0216	1.2002	0.0000	1.2314	0.0000	1.3046	0.0134	1.2018	0.0994
2149.8.....	1.0403	0.0196	1.2025	0.0000	1.2322	0.0000	1.3051	0.0123	1.1971	0.0953
2150.3.....	1.0560	0.0196	1.2047	0.0000	1.2330	0.0000	1.3060	0.0106	1.1879	0.0882
2150.8.....	1.0676	0.0203	1.2068	0.0000	1.2337	0.0000	1.3068	0.0097	1.1806	0.0789
2151.3.....	1.0772	0.0203	1.2088	0.0000	1.2343	0.0000	1.3073	0.0089	1.1771	0.0690
2151.8.....	1.0875	0.0194	1.2106	0.0000	1.2347	0.0000	1.3080	0.0076	1.1736	0.0577
2152.2.....	1.0909	0.0180	1.2121	0.0000	1.2353	0.0000	1.3084	0.0066	1.1746	0.0478
2152.7.....	1.1007	0.0165	1.2135	0.0000	1.2358	0.0000	1.3093	0.0054	1.1759	0.0382
2153.2.....	1.1080	0.0159	1.2148	0.0000	1.2363	0.0000	1.3102	0.0042	1.1786	0.0299
2153.7.....	1.1151	0.0141	1.2161	0.0000	1.2367	0.0000	1.3112	0.0032	1.1822	0.0227
2154.2.....	1.1224	0.0127	1.2173	0.0000	1.2372	0.0000	1.3125	0.0022	1.1876	0.0171
2154.7.....	1.1302	0.0133	1.2183	0.0000	1.2375	0.0001	1.3139	0.0017	1.1890	0.0122
2155.1.....	1.1324	0.0133	1.2194	0.0000	1.2379	0.0000	1.3146	0.0013	1.1953	0.0089
2156.1.....	1.1440	0.0119	1.2213	0.0000	1.2386	0.0001	1.3170	0.0009	1.2042	0.0046
2157.1.....	1.1536	0.0113	1.2229	0.0000	1.2392	0.0002	1.3185	0.0011	1.2117	0.0026
2158.0.....	1.1607	0.0102	1.2244	0.0002	1.2397	0.0002	1.3197	0.0002	1.2170	0.0018
2159.0.....	1.1700	0.0114	1.2256	0.0001	1.2402	0.0002	1.3217	0.0003	1.2218	0.0015
2160.0.....	1.1759	0.0122	1.2268	0.0002	1.2405	0.0002	1.3230	0.0003	1.2251	0.0015
2160.9.....	1.1800	0.0102	1.2278	0.0002	1.2410	0.0003	1.3241	0.0004	1.2284	0.0015
2161.9.....	1.1866	0.0085	1.2289	0.0001	1.2413	0.0003	1.3252	0.0003	1.2311	0.0015
2162.9.....	1.1939	0.0099	1.2300	0.0002	1.2416	0.0003	1.3263	0.0000	1.2331	0.0015
2163.8.....	1.1955	0.0112	1.2308	0.0004	1.2419	0.0004	1.3276	0.0002	1.2352	0.0015
2164.8.....	1.1999	0.0083	1.2316	0.0004	1.2421	0.0003	1.3284	0.0005	1.2371	0.0015
2165.7.....	1.2044	0.0090	1.2322	0.0004	1.2424	0.0003	1.3293	0.0001	1.2384	0.0015
2166.7.....	1.2074	0.0112	1.2331	0.0005	1.2426	0.0003	1.3305	0.0004	1.2401	0.0015
2167.7.....	1.2099	0.0080	1.2336	0.0006	1.2428	0.0003	1.3313	0.0004	1.2415	0.0015
2168.6.....	1.2145	0.0077	1.2341	0.0006	1.2430	0.0003	1.3322	0.0004	1.2425	0.0015
2169.6.....	1.2183	0.0095	1.2348	0.0004	1.2432	0.0003	1.3329	0.0005	1.2435	0.0016
2172.0.....	1.2232	0.0094	1.2360	0.0008	1.2437	0.0002	1.3355	0.0003	1.2459	0.0015
2174.4.....	1.2290	0.0094	1.2370	0.0010	1.2441	0.0002	1.3374	0.0004	1.2478	0.0016
2176.8.....	1.2352	0.0115	1.2380	0.0008	1.2444	0.0002	1.3396	0.0003	1.2494	0.0016
2179.2.....	1.2363	0.0097	1.2384	0.0014	1.2447	0.0002	1.3420	0.0000	1.2506	0.0015
2181.7.....	1.2416	0.0116	1.2392	0.0013	1.2450	0.0001	1.3445	0.0003	1.2518	0.0016
2184.1.....	1.2449	0.0114	1.2396	0.0014	1.2453	0.0001	1.3467	0.0004	1.2531	0.0016
2186.5.....	1.2461	0.0118	1.2399	0.0014	1.2454	0.0000	1.3492	0.0000	1.2539	0.0015
2188.9.....	1.2486	0.0131	1.2405	0.0015	1.2457	0.0000	1.3519	0.0002	1.2547	0.0015
2191.3.....	1.2472	0.0120	1.2410	0.0016	1.2459	0.0001	1.3543	0.0000	1.2554	0.0014
2193.7.....	1.2532	0.0068	1.2412	0.0016	1.2461	0.0001	1.3572	0.0001	1.2562	0.0014
2196.1.....	1.2563	0.0122	1.2414	0.0018	1.2463	0.0001	1.3599	0.0003	1.2567	0.0015
2204.3.....	1.2592	0.0151	1.2421	0.0018	1.2467	0.0000	1.3691	0.0000	1.2584	0.0013
2211.5.....	1.2573	0.0144	1.2422	0.0014	1.2471	0.0000	1.3790	0.0002	1.2594	0.0013
2219.7.....	1.2587	0.0101	1.2423	0.0012	1.2474	0.0000	1.3912	0.0005	1.2603	0.0012
2227.9.....	1.2581	0.0072	1.2428	0.0000	1.2476	0.0001	1.4057	0.0000	1.2611	0.0010
2236.1.....	1.2649	0.0008	1.2439	0.0000	1.2478	0.0001	1.4212	0.0004	1.2617	0.0008

physical context. The spectra in Tielens et al. (1991) and Chiar et al. (1994, 1995) show that the 2140 cm<sup>-1</sup> component usually dominates the interstellar absorption feature associated with frozen CO along most lines of sight. In addition to this feature, all lines of sight also have some contribution from the 2135 cm<sup>-1</sup> band which is associated with CO in H<sub>2</sub>O-rich ices. In the following sections we compare the interstellar CO feature, especially the 2140 cm<sup>-1</sup> component, with those of the laboratory analogs described above and use these comparisons to place constraints on the interstellar ice composition. Figures 12 and 13 show interstellar CO bands representative of the features that must be matched. The astronomical spectra in these figures are taken from Tielens et al. (1991). *Comparisons between the astronomical and laboratory spectra are made in transmittance, not optical depth units as is customary, in order to facilitate comparison across the entire feature.*

#### 4.1. N<sub>2</sub>:CO Ices

The data in Table 2 and Figure 1 show that the position and width of the CO feature depends upon the ratio of N<sub>2</sub> to CO in these ices. Comparison of the N<sub>2</sub>:CO ice spectra with the interstellar CO features given in Figures 12 and 13 show that while the more dilute mixtures (N<sub>2</sub>:CO = 25:1 and 100:1) match the position of the interstellar peak reasonably well, they are far too narrow (1.0–1.3 cm<sup>-1</sup> versus a more typical width of ~10 cm<sup>-1</sup> for the interstellar band). In the N<sub>2</sub>:CO = 2:1 and 1:20 ices, the peak frequency is too low by about 1 cm<sup>-1</sup> and the width is still too narrow (between 2 and 3 cm<sup>-1</sup>). This trend is consistent with the 0.18–0.013 cm<sup>-1</sup> line widths reported by Dubost, Charneau, & Harig (1982) for CO in N<sub>2</sub> matrices at mole fractions of 10<sup>-2</sup> to 10<sup>-5</sup>, respectively. The mismatches in position and width are not improved by warming (Fig. 2,

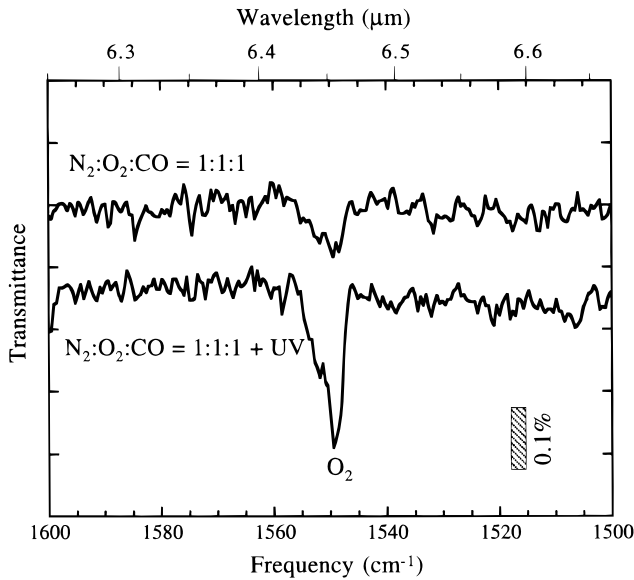


FIG. 11.—The  $\text{O}_2$  stretching band produced by an  $\text{N}_2:\text{O}_2:\text{CO} = 1:1:1$  ice at 12 K before (*upper trace*) and after (*lower trace*) UV irradiation. Band strength enhancement is presumably due to the introduction of additional irregularities into the ice structure by photolysis.

Table 2) or photolysis (Table 6). These experiments also demonstrate that in order for interstellar (and cometary) ices to contain appreciable amounts of  $\text{N}_2$ , they must remain well below 30 K (see Fig. 2).

In summary, while the band positions are consistent with the hypothesis that CO can be frozen along with  $\text{N}_2$  in these interstellar clouds, this series shows that ices made solely of

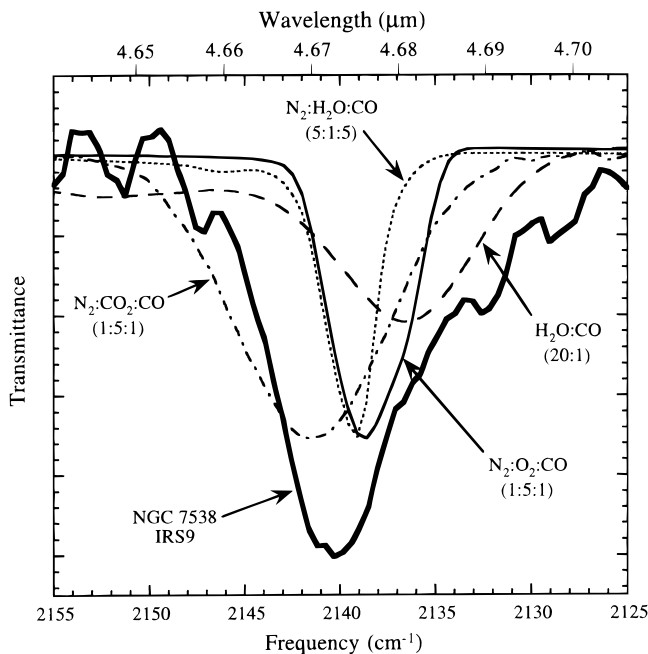


FIG. 12.—Comparison between the solid CO ice in the spectrum of NGC 7538 IRS 9 (*thick solid line*; taken from Tielens et al. 1991) and the features produced by the ices  $\text{H}_2\text{O}:\text{CO} = 20:1$ ,  $\text{N}_2:\text{O}_2:\text{CO} = 1:5:1$ ,  $\text{N}_2:\text{H}_2\text{O}:\text{CO} = 5:1:5$ , and  $\text{N}_2:\text{CO}_2:\text{CO} = 1:5:1$  at 12 K (*various thin lines*). This demonstrates that (i)  $\text{H}_2\text{O}$ -rich ices can reproduce the  $2135\text{ cm}^{-1}$  component of the interstellar feature, (ii) the features produced by nonpolar ices dominated by  $\text{N}_2$  and  $\text{O}_2$  are too narrow and fall  $\sim 1\text{ cm}^{-1}$  to the red, and (iii) the added presence of  $\text{CO}_2$  produces dramatic increases in the width and frequency of the band.

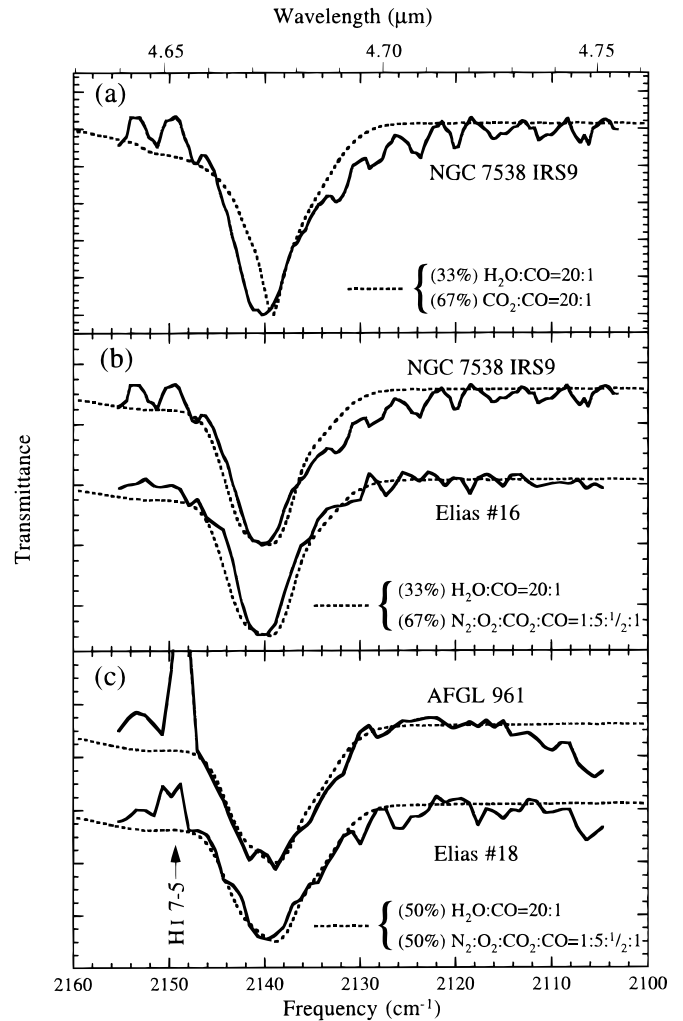


FIG. 13.—Comparison between the solid CO ice feature in the spectra of NGC 7538 IRS 9, AFGL 961, Elias 16, and Elias no. 18 (*thick solid lines*; taken from Tielens et al. 1991) and the features produced by co-adding bands from two ice analogs (*dotted lines*). Fits were obtained by co-adding differing amounts of absorption due to CO in a nonpolar ice and CO in a polar ( $\text{H}_2\text{O}:\text{CO} = 20:1$ ) ice. (a) The fit provided to the spectrum of NGC 7538 IRS 9 by a combination of  $\text{CO}_2:\text{CO} = 20:1$  (67%) and  $\text{H}_2\text{O}:\text{CO} = 20:1$  (33%) ices. This fit requires too much cosmic C be in the form of  $\text{CO}_2$ , fails to match the interstellar band position, and does not account for the high-frequency wing of the interstellar feature. (b) The fit provided to the spectra of NGC 7538 IRS 9 and Elias no. 16 by a combination of  $\text{N}_2:\text{O}_2:\text{CO}_2:\text{CO} = 1:5:\frac{1}{2}:1$  (67%) and  $\text{H}_2\text{O}:\text{CO} = 20:1$  (33%) ices. (c) The fit provided to the spectra of AFGL 961 and Elias no. 18 by a combination of  $\text{N}_2:\text{O}_2:\text{CO}_2:\text{CO} = 1:5:\frac{1}{2}:1$  (50%) and  $\text{H}_2\text{O}:\text{CO} = 20:1$  (50%) ices. Co-adds with the  $\text{N}_2:\text{O}_2:\text{CO}_2:\text{CO} = 1:5:\frac{1}{2}:1$  ice produce a much better fit. Higher proportions of the polar,  $\text{H}_2\text{O}$ -rich ice component are required for the embedded objects AFGL 961 and Elias 18, suggesting that these lines of sight sample the vicinities of newly forming stars where the interstellar ices may be partially “distilled” of their more volatile, nonpolar components.

CO and  $\text{N}_2$  do not fit the interstellar feature in a satisfactory manner because they produce bands that are too narrow.

#### 4.2. $\text{N}_2:\text{H}_2\text{O}:\text{CO}$ Ices

The addition of a third plausible component to the  $\text{N}_2:\text{CO}$  mixtures improves the situation somewhat. Given that  $\text{H}_2\text{O}$  is the most abundant molecule frozen on interstellar grains, it is a logical third component to consider. The spectral properties of the CO band produced by  $\text{N}_2:\text{H}_2\text{O}:\text{CO}$  ices are shown in Figure 3 and summarized

in Table 3. The CO peak frequencies of these ices span the range from 2139.7 to 2139.1 cm<sup>-1</sup> and consistently match the interstellar peak position better than those of the binary N<sub>2</sub>:CO mixtures. In addition, the bands are broader and their widths best match that of the interstellar feature when the concentrations of N<sub>2</sub>, H<sub>2</sub>O, and CO are comparable. Of the mixtures we have studied, the N<sub>2</sub>:H<sub>2</sub>O:CO = 2:1:1 ice, having a peak position of 2139.2 cm<sup>-1</sup> and a FWHM of 5.3 cm<sup>-1</sup>, produces a CO feature which comes the closest of these ices to matching the 10 cm<sup>-1</sup> wide interstellar band (Table 3 and Fig. 12). The data listed in Tables 3 and 6 show that the CO feature in these trinary mixtures is not altered much by photolysis or warming over the entire range of temperatures at which the N<sub>2</sub> ice is stable.

However, a broad feature near 2148 cm<sup>-1</sup>, absent from the interstellar spectra, is also produced in many of the ices which contain H<sub>2</sub>O. It is most intense when the H<sub>2</sub>O concentration is high, and becomes almost unobservable at very low H<sub>2</sub>O concentrations (Fig. 3, Table 3). The ices which produce the best fits to the 2140 cm<sup>-1</sup> interstellar feature have some of the strongest 2148 cm<sup>-1</sup> bands. Since this second band always appears in the spectra of ices containing substantial amounts of H<sub>2</sub>O, and it is not evident in the interstellar spectra (although telluric obscuration and overlapping gas-phase CO rotational bands plus the H 1 7–5 transition make it difficult to detect this feature), we rule out ices in which the H<sub>2</sub>O concentration is comparable to, or greater than, that of the other nonpolar components as carriers of the 2140 cm<sup>-1</sup> band. Conversely, while lower H<sub>2</sub>O concentrations such as that in the N<sub>2</sub>:H<sub>2</sub>O:CO = 5:1:5 ice do not show a 2148 cm<sup>-1</sup> band (Figs. 3 and 12) and produce a CO band which comes close to the interstellar peak frequency, they are too narrow and fall ~1 cm<sup>-1</sup> to the red of the interstellar position (see Fig. 12). Thus, mixtures which contain *minor* amounts of polar molecules but which are dominated by nonpolar species could contribute to the interstellar feature, but cannot fully explain it.

#### 4.3. O<sub>2</sub>:CO, CO<sub>2</sub>:CO, N<sub>2</sub>:O<sub>2</sub>:CO, and N<sub>2</sub>:CO<sub>2</sub>:CO Ices

The data in Table 4 and Figures 4 and 5 show that simple binary mixtures of O<sub>2</sub>:CO, and CO<sub>2</sub>:CO cannot reproduce the peak position, FWHM, and profile of the interstellar feature. In the case of O<sub>2</sub>:CO, the position is too low by about 3 cm<sup>-1</sup> and the band too narrow by about 5 cm<sup>-1</sup>. Although the CO<sub>2</sub>:CO = 20:1 mixture has been used to fit the interstellar feature in the past, it too is inadequate since it has a high-frequency wing not seen in the interstellar band profile.

While an O<sub>2</sub>:CO = 20:1 mixture does not match the position or width of the interstellar feature, three-component N<sub>2</sub>:O<sub>2</sub>:CO mixtures do a bit better. Both the N<sub>2</sub>:O<sub>2</sub>:CO = 1:1:1 and 1:5:1 mixtures have CO features which peak about 1–2 cm<sup>-1</sup> to the red and are too narrow by several cm<sup>-1</sup> (see Fig. 12). Table 6 shows that photolysis does not alter the frequency to better match the interstellar band position, and, although it increases the width of the CO feature in the N<sub>2</sub>:O<sub>2</sub>:CO = 1:1:1 ice from 4.0 cm<sup>-1</sup> to 6.0 cm<sup>-1</sup>, it is still too narrow.

A similar study of the influence of CO<sub>2</sub> on the CO band in N<sub>2</sub>:CO ices leads to the following conclusions. In the lowest concentration case (N<sub>2</sub>:CO<sub>2</sub>:CO = 1:1:1), the CO band is blueshifted into closer agreement with the inter-

stellar band by nearly 1 cm<sup>-1</sup>, but it remains far too narrow. Higher concentrations of CO<sub>2</sub> produce even more widening and blueshifting of the band. The N<sub>2</sub>:CO<sub>2</sub>:CO = 1:5:1 ice has a CO feature that is broadened to a FWHM of 9.6 cm<sup>-1</sup> (see Fig. 12) and blueshifted by 2 cm<sup>-1</sup> to 2141.5 cm<sup>-1</sup>, a frequency 1 cm<sup>-1</sup> too *high* for the interstellar feature. The CO<sub>2</sub>, which is too large to fit into the N<sub>2</sub> lattice, presumably breaks up the regularity of the N<sub>2</sub> matrix, causing the band to shift slightly to the blue and adding extra absorbance to the high-frequency wing of the feature.

The principal conclusions from the best fits to the interstellar feature found in this and the previous two sections can be summarized by examining Figure 12. Three-component nonpolar ices such as N<sub>2</sub>:O<sub>2</sub>:CO = 1:5:1, or nonpolar ices with a low concentration of a polar species such as H<sub>2</sub>O (N<sub>2</sub>:H<sub>2</sub>O:CO = 5:1:5), produce features which peak near 2139 cm<sup>-1</sup>, approximately 1 cm<sup>-1</sup> to the red of the interstellar peak position. In both cases, the bands are too narrow, do not reproduce the peak position, and fail to account for the absorption on the high-frequency side of the interstellar band. Of all the possible components studied here, CO<sub>2</sub> is the *only* one which can shift the CO absorption to frequencies up to and *higher* than the interstellar band peak position. This behavior suggests that an improved fit to the interstellar feature might best be provided by adding some CO<sub>2</sub> to ices like N<sub>2</sub>:O<sub>2</sub>:CO = 1:5:1, or possibly N<sub>2</sub>:H<sub>2</sub>O:CO = 5:1:5. This possibility is discussed below.

#### 4.4. N<sub>2</sub>:O<sub>2</sub>:CO<sub>2</sub>:CO Ices

The spectra in Figure 6 and data in Table 4 show the CO feature in ices made up of N<sub>2</sub>, O<sub>2</sub>, CO<sub>2</sub>, and CO. The results of these four-component ice experiments show that the roles played by the individual components in simpler ices are maintained, i.e., the N<sub>2</sub> and O<sub>2</sub> in the ices result in CO absorption centered near 2139 cm<sup>-1</sup>, while the presence of CO<sub>2</sub> produces absorption above 2140 cm<sup>-1</sup>. The best match to the interstellar feature is provided by N<sub>2</sub>:O<sub>2</sub>:CO<sub>2</sub>:CO = 1:5:½:1. Ices with higher CO<sub>2</sub> concentrations produce too large a blueshift and too much absorption on the high-frequency side of the band.

Figure 13 compares the profile of the CO ice feature of several laboratory ices with the spectra along four lines of sight through interstellar clouds. We have followed the common practice of fitting the entire interstellar feature with the combined absorption resulting from two different ice components. The first component, H<sub>2</sub>O:CO = 20:1, is added to account for the lower frequency 2135 cm<sup>-1</sup> band produced by CO frozen in highly polar matrices (Sandford et al. 1988). This is only a minor component along most lines of sight (Tielens et al. 1991; Chiar et al. 1994, 1995). The second, and dominant, component is that of CO in a nonpolar ice and it is added to provide the deeper, narrower 2140 cm<sup>-1</sup> feature. In Figure 13a, we show the best fit that can be obtained to the spectrum of NGC 7538 IRS 9 using H<sub>2</sub>O:CO = 20:1 as the polar component and CO<sub>2</sub>:CO = 20:1 as the nonpolar component. While these two components have been used to fit interstellar data in the past, it is clear that this can be improved upon. In Figures 13b and 13c we show comparisons to the spectra of NGC 7538 IRS 9, Elias 16, AFGL 961, and Elias 18 where the CO<sub>2</sub>:CO = 20:1 nonpolar component is replaced with that of the N<sub>2</sub>:O<sub>2</sub>:CO<sub>2</sub>:CO = 1:5:½:1 ice (see Fig. 6). The fits utilizing the four-component ice are considerably better across

the entire feature. On the basis of these greatly improved fits we conclude that an interstellar ice composition which best reproduces the  $2140\text{ cm}^{-1}$  CO band characteristic of the quiescent regions of dense molecular clouds is one in which  $\text{O}_2$  is important (comparable to or a few times more abundant than CO), the  $\text{N}_2$  concentration is comparable to that of the CO, and the  $\text{CO}_2$  concentration is less than that of the CO.

### 5. ASTROPHYSICAL IMPLICATIONS

The results and analysis of the experiments described above will now be used to draw conclusions regarding the composition of interstellar ices in quiescent regions of dense molecular clouds. As pointed out by Tielens et al. (1991) and Chiar et al. (1994, 1995), the solid CO spectral characteristics of the lines of sight which probe the quiescent portions of molecular clouds can be quite distinct from those closely associated with embedded protostars. For example, the  $2140\text{ cm}^{-1}$  component of the CO feature which is associated with nonpolar ices is dominant toward field stars behind the Taurus molecular cloud and many other embedded objects, whereas it is less than or comparable in strength to the  $2135\text{ cm}^{-1}$  component associated with CO trapped in  $\text{H}_2\text{O}$ -rich ices toward the embedded protostellar object W33 A. This suggests that the  $2135\text{ cm}^{-1}$  band, and other unique characteristics of the spectrum toward W33 A, such as the prominent XCN and  $\text{CH}_3\text{OH}$  bands, are to be associated more with the environment of the protostar than with the molecular cloud itself. Perhaps in those cases in which the  $2135\text{ cm}^{-1}$  component is more dominant, the lines of sight sample "distilled" ices in higher density material surrounding the protostar, perhaps material in the disk. In general, lines of sight to background stars typically show a CO feature which is somewhat narrower than those associated with embedded objects and require smaller contributions from the polar component (Fig. 13), consistent with this possibility. However, even the spectra of background sources, such as Elias 16 (Fig. 13*b*), require some contribution from the  $2135\text{ cm}^{-1}$  band of polar ices. This implies that  $\text{H}_2\text{O}$ -rich ices are present in the quiescent regions of the cloud as well, but they are less important.

This overall behavior is consistent with the picture that the ices in the protostellar environment probed have probably undergone substantially more radiative processing and are somewhat warmer (i.e., well above 30 K) than those ices along lines of sight which have more obscuration arising in quiescent regions. At these warmer temperatures, the nonpolar ices discussed here cannot survive, whereas  $\text{H}_2\text{O}$ -rich mixtures can. Therefore, throughout the following discussion we assume that the CO profile contains contributions from both nonpolar and  $\text{H}_2\text{O}$ -rich polar ices, with the nonpolar component dominating in the quiescent regions. As shown in Sandford et al. (1988), a nonpolar ice deposited on top of a polar ice does not affect the band position of either component. Thus the results presented here can arise from the nonpolar and polar ices being present as various layers on the same grain, or present on different grains.

We do not take Doppler shifts or scattering and grain size distributions into account. Doppler shifts can account for between 0.3 to at most  $1.0\text{ cm}^{-1}$  shifts for the data considered here. Since this uncertainty is on the order of the quality of the fit across the entire band shown in Figures 12 and 13, corrections at this precision are not currently warranted. Scattering and size distribution effects can also alter the bands (Tielens et al. 1991). However, since the matches

already presented are quite good, we will leave this level of analysis to others, using the optical constants presented in § 3.3.

The preceding arguments point to a picture where the  $2140\text{ cm}^{-1}$  band arises from the densest regions of molecular clouds where the production of nonpolar species such as  $\text{O}_2$ ,  $\text{N}_2$ , and CO are favored over polar species such as  $\text{H}_2\text{O}$ . On the other hand, there are at least two distinct regions which can produce  $\text{H}_2\text{O}$ -rich ices and the  $2135\text{ cm}^{-1}$  band. In the cloud regions where the  $\text{H}/\text{H}_2$  ratio is above unity, the production of hydrogenated species such as  $\text{H}_2\text{O}$  is favored over the production of nonpolar species on grain surfaces (Tielens & Hagen 1982; d'Hendecourt, Allamandola, & Greenberg 1985). Here, provided the grains are cold enough, CO and other simple nonpolar species can be frozen in the  $\text{H}_2\text{O}$  because the  $\text{H}_2\text{O}$ -CO binding energy is substantially greater than the CO-CO binding energy (e.g., Sandford & Allamandola 1990a).  $\text{H}_2\text{O}$ -rich ices can also be produced in the warm protostellar regions by the "distillation" of interstellar ices. In this case, the  $\text{H}_2\text{O}$ -rich ices will not be the result of an ongoing, continuous process, but rather they will be all that remains as the ices warm and the more volatile, nonpolar species sublime. Consequently, these  $\text{H}_2\text{O}$ -rich ices are most probably different in character from those produced in the  $\text{H}/\text{H}_2 > 1$  regions within the body of the cloud. The prominence of spectral features arising from species such as XCN and  $\text{CH}_3\text{OH}$  toward W33 A suggest that most of the extinction toward this object arises from a very dense, warm region close to the source. Here, various processes including UV photolysis will drive different chemistry from that in the quiescent cloud regions and these  $\text{H}_2\text{O}$ -rich ices and their photoproducts (Bernstein et al. 1995) are likely to be important feedstock species in protostellar nebulae. Charnley (1996) has recently developed an interesting model of the gas-grain chemistry in these regions. Thus it appears that the chemical conditions in some protostellar nebula are different from those considered in many models of the solar nebula which assume that most of the C is in CO and  $\text{CH}_4$ , and not  $\text{CH}_3\text{OH}$  (Pollack et al. 1994).

#### 5.1. Interstellar $\text{N}_2$ and $\text{O}_2$ Abundances and Depletions

In order to avoid confusion with contributions from the species in the polar,  $\text{H}_2\text{O}$ -rich fraction of the ice, we restrict the following discussion to the nonpolar component in quiescent regions of dense clouds. We believe that this provides a reasonable measure of the nonpolar species' abundance along the entire line of sight since depletions of significant amounts (more than 10%) of nonpolar species diluted in the  $\text{H}_2\text{O}$ -rich component can be ruled out by the absence of a prominent high-frequency feature near  $2150\text{ cm}^{-1}$  in the interstellar spectra (§ 4.2).

The calculations described below are based on a nonpolar interstellar ice composition of  $\text{N}_2:\text{O}_2:\text{CO}_2:\text{CO} = 1:5:\frac{1}{2}:1$ . We have selected this composition because it provides a good fit to the interstellar feature (see § 4.4) and because it has molecular abundances that are similar to those predicted for quiescent cloud environments by the early chemical models which took both gas-phase and ice grain processes into account. For example, the time-dependent treatment of d'Hendecourt, Allamandola, & Greenberg (1985) predicted grain mantles dominated by  $\text{O}_2$  (43%), CO (30%),  $\text{N}_2$  (10%), and  $\text{CO}_2$  (8%) in the high-density, high-extinction regions of dense clouds. Similarly,

the equilibrium treatment of Tielens & Hagen (1982) predicted a mantle composition of roughly 58% O<sub>2</sub>, 40% CO, and a few percent of CO<sub>2</sub>, H<sub>2</sub>O, and N<sub>2</sub> in the highest density regions. While these models were quite simple by today's standards, the observations support the basic assumptions involved and will hopefully encourage the inclusion of species such as N<sub>2</sub> and O<sub>2</sub> in the more sophisticated current treatments.

N<sub>2</sub>, O<sub>2</sub>, and CO<sub>2</sub> are certainly not the only potentially important nonpolar interstellar species in these cloud regions. H<sub>2</sub> is likely to be orders of magnitude more abundant than any of the molecules considered here. We rule out H<sub>2</sub> as playing an important role in these nonpolar ices for two reasons. First, it is too volatile. While H<sub>2</sub> has been detected frozen in H<sub>2</sub>O-rich interstellar ices (Sandford et al. 1993), its binding energy to these nonpolar species is such that it would not condense in significant amounts on interstellar grain surfaces. Second, even if some were trapped in these ices, it would not perturb the lattice sufficiently to produce the band broadening required since it is smaller than N<sub>2</sub>, O<sub>2</sub>, and CO<sub>2</sub>. Another plausible species is CH<sub>4</sub>. Absorption attributed to frozen CH<sub>4</sub> has been detected toward NGC 7538 IRS 9 and possibly toward W33 A and NGC 7538 IRS 1 (Lacy et al. 1991). It may even be comparable in abundance to solid CO. Nonetheless, we rule this out as a significant player since it seems the highest abundances with respect to frozen CO are along lines of sight mostly associated with H<sub>2</sub>O-rich ices such as W33 A. The clearest detection is toward NGC 7538 IRS 9, and here the ratio of solid CO to solid CH<sub>4</sub> is 8. Observations probing the abundance of frozen CH<sub>4</sub> relative to that of frozen H<sub>2</sub>O and CO along several other lines of sight toward embedded

objects and background stars will place important additional constraints on the ice composition and chemistry of these two regions. Interestingly, Sandford et al. (1988) show that when CH<sub>4</sub> is the dominant constituent, the CO feature falls at 2137 cm<sup>-1</sup>, close to the position in H<sub>2</sub>O-rich ices. It is too narrow (FWHM = 2–3 cm<sup>-1</sup>), however, to account for the interstellar feature associated with the polar-component.

Table 9 presents estimates of the O<sub>2</sub> and N<sub>2</sub> solid state column densities and abundances relative to H along the lines of sight to several embedded objects and background field stars. The column densities were derived from those of solid CO, assuming that the ratio of N<sub>2</sub>:O<sub>2</sub>:CO<sub>2</sub>:CO is equal to 1:5:½:1. It should be kept in mind that these assumed relative abundances serve as approximations only. While the relative concentration of CO<sub>2</sub> is fairly well constrained by our spectral matches (any more and it produces a feature that is too broad and too blue), the relative amounts of N<sub>2</sub> and O<sub>2</sub> are not as strongly constrained. For example, our four-component ices contain somewhat more O<sub>2</sub> than predicted would be present based on the simple models of Tielens & Hagen (1982) and d'Hendecourt et al. (1985), and our experiments do not preclude the possibility that ices containing smaller amounts of O<sub>2</sub> can still provide a good fit to the interstellar feature. The H abundances were calculated from the standard dust-to-gas conversion  $N_H = A_v (1.9 \times 10^{21} \text{ cm}^{-2} \text{ mag}^{-1})$ , using extinction ( $A_v$ ) values published for these objects. The cosmic abundance values, in units of ppm with respect to H, which were adopted for this calculation are O = 480, N = 60, and C = 250. These numbers take into consideration the recent cosmic abundance revisions reported by Snow & Witt (1995), Mathis

TABLE 9

COLUMN DENSITIES OF SOLID CO IN NONPOLAR INTERSTELLAR ICES AND THE PERCENT OF COSMIC NITROGEN AND OXYGEN IN THE FORM OF FROZEN N<sub>2</sub> AND O<sub>2</sub> IN THE QUIESCENT REGIONS OF DENSE MOLECULAR CLOUDS

Object	$N(\text{H})$ ( $\times 10^{22} \text{ cm}^{-2}$ )	$N(\text{CO})_{\text{nonpolar}}$ ( $\times 10^{17} \text{ cm}^{-2}$ )	%N in Solid N <sub>2</sub>	%O in Solid O <sub>2</sub>
Taurus				
Elias 1 (em) <sup>a</sup> .....	1.7 <sup>b</sup>	0.5 <sup>a</sup>	9.7	6
Elias 3 (bkgd) <sup>a</sup> .....	1.6 <sup>b</sup>	1.7 <sup>a</sup>	37	23
Elias 13 (bkgd) <sup>a</sup> .....	2.0 <sup>b</sup>	0.9 <sup>a</sup>	15	9.5
Elias 16 (bkgd) <sup>a</sup> .....	4.2 <sup>b</sup>	5.6 <sup>a</sup>	43	27
Elias 18 (em) <sup>a</sup> .....	3.5 <sup>b</sup>	1.6 <sup>a</sup>	15	9.5
Tamura 8 (bkgd) <sup>a</sup> .....	3.5 <sup>b</sup>	4.7 <sup>a</sup>	43	27
Serpens				
CK 1 (bkgd?) <sup>c</sup> .....	2.9 <sup>b</sup>	6.5 <sup>d</sup>	73	46
CK 2 (bkgd) <sup>c</sup> .....	8.7 <sup>b</sup>	10	40	25
CK 3 (bkgd?) <sup>c</sup> .....	1.8 <sup>b</sup>	0.87	16	10
SVS 4 (bkgd?) <sup>c</sup> .....	4.8 <sup>b</sup>	2.3	16	10
SVS 9 (bkgd?) <sup>c</sup> .....	2.8 <sup>b</sup>	<2.6	30	19
Miscellaneous				
NGC 7538 IRS 9 (em).....	16 <sup>c</sup>	6.4 <sup>c</sup>	13	8.5
L1551 IRS 5 (em) .....	2.3 <sup>c</sup>	2.3 <sup>c</sup>	33	21
W33 A (em).....	2.8 <sup>c</sup>	1.1 <sup>c</sup>	1.3	1
AFGL 961 (em) .....	7.4 <sup>c</sup>	1.5 <sup>c</sup>	6.7	4
NGC 2024 IRS 2 (em).....	6.0 <sup>c</sup>	1.2 <sup>c</sup>	6.7	4

NOTE.—(em) ⇒ object is embedded in the molecular cloud; (bkgd) ⇒ object is behind the molecular cloud.

<sup>a</sup> From Chiar et al. 1995.

<sup>b</sup> Calculated from  $A_v$  as described in § 5.1.

<sup>c</sup> From Chiar et al. 1994.

<sup>d</sup> Assumes all CO is in a nonpolar ice; see Eiroa & Hodapp 1989.

<sup>e</sup> From Tielens et al. 1991.

(1996), and Cardelli et al. (1996).

Within the framework of the assumptions described above, the abundances listed in the table indicate that available interstellar N in the form of frozen  $N_2$  along the lines of sight probed toward background stars lies in the 15%–70% range, with an average of about 35%. For the embedded objects, this is reduced to a range of 1%–30% with an average of about 10%.  $N_2$  and CO are likely to have similar gas/grain distributions in the quiescent regions because they have similar heats of vaporization and  $N_2$  is unreactive. Thus, since approximately 40% of the CO is depleted onto grains in quiescent cloud regions (Chiar et al. 1994, 1995), a similar relationship probably holds for  $N_2$ . Therefore, in the quiescent regions where an average of 35% of the available N is in frozen  $N_2$ , the implication is that as much as 70% of the total available N is in  $N_2$  (gas + ice).

The amount of O tied up in frozen  $O_2$  lies in the 1%–45% range toward background sources (average = 20%), and lies between 1% and 20% for embedded objects (average = 10%). The amount of oxygen tied up in frozen CO and  $CO_2$  in the nonpolar ices lies between 2% and 10% of the total O in quiescent regions, and on the order of 0.2%–5% for lines of sight toward embedded objects. Since nearly 40% of the total amount of O available is thought to be tied up in refractory grain materials such as silicates (Cardelli et al. 1996), this implies that nearly half of the O available in the gas could be tied up in  $O_2$  along some lines of sight (recall that the estimates for  $O_2$  are likely to be upper limits, see above)].

Lastly, these calculations imply that the fraction of carbon tied up in frozen CO and  $CO_2$  in the nonpolar ices lies in the 3%–13% range toward field stars and between 0.2% and 6% toward embedded objects.

Keep in mind that our assumed nonpolar composition of  $N_2:O_2:CO_2:CO = 1:5:\frac{1}{2}:1$  is probably not unique with regards to its ability to fit the interstellar CO feature. Similar quality fits to the interstellar feature can probably be made with a range of nonpolar compositions. For example, the features produced by  $N_2:O_2:CO = 1:5:1$  and  $N_2:H_2O:CO = 5:1:5$  ices (see Fig. 12) suggest that it is possible that minor amounts of  $H_2O$  may carry out the same spectral function as larger amounts of  $O_2$ . Thus, it might be possible to obtain a comparably good fit to the interstellar feature by replacing the  $N_2:O_2:CO_2:CO = 1:5:\frac{1}{2}:1$  nonpolar component with an ice of the form  $N_2:H_2O:CO_2:CO$ . Thus, the cosmic abundances summarized in Table 8 should not be taken as exact, but should serve as a guide only. Furthermore, the previous discussion relates only to the cosmic abundance contributions made by the *nonpolar* fraction of the CO-bearing ices. The *polar*  $H_2O$ -rich ice component will also provide significant contributions to the cosmic inventory. As shown in Figure 13, the contribution of C and O due to the polar ices can be comparable to those from the nonpolar ices, especially along lines of sight toward embedded objects.

In summary, based on the assumption that the  $2140\text{ cm}^{-1}$  CO band is produced by a nonpolar ice having a composition of  $N_2:O_2:CO_2:CO = 1:5:\frac{1}{2}:1$ , it appears that most of the interstellar N and a significant fraction of the interstellar O in the quiescent regions of dense molecular clouds are in the form of  $N_2$  and  $O_2$ . These two molecular components appear to be far more important ice species in quiescent regions of the cloud than along lines of sight to embedded objects. Given that the spectra of embedded

objects also contain variable, but significant, spectral contributions from foreground quiescent cloud material, but still show substantial reductions in implied  $N_2$  and  $O_2$ , suggests that the ices in the vicinity of embedded objects are significantly different from those in more typical regions in dense clouds.

This may also have some implications for our understanding of the conditions in the solar nebula and the composition of icy bodies at large distances from the protostar. For example, if these objects were formed at large enough distances that the temperatures never rose much above 30 K, these icy planetesimals might well contain significant amounts of  $N_2$  and  $O_2$ . Cometary outbursts at large heliocentric distances such as that recently reported for comet Hale-Bopp are often attributed to the release of volatiles such as CO (Jewitt, Senay, & Matthews 1996; Sekanina 1996). If comets contain some of the interstellar ices that were present prior to the formation of the solar system,  $O_2$  and  $N_2$  should certainly be present. These too should be considered, as they will also drive releases at low temperatures.

### 5.2. Photoproducts of Nonpolar Ices

Since  $N_2$ ,  $O_2$ , and  $CO_2$  are likely to be important interstellar ice components, the products formed by the energetic processing of these ices are of interest. The results presented in § 3.2 show that  $N_2O$ ,  $O_3$ , and  $CO_3$  might also be important interstellar ice components in cold ( $T < 30\text{ K}$ ) regions exposed to radiation. Figures 8 and 9 show that the strongest  $N_2O$  bands fall near  $2235$  and  $1291\text{ cm}^{-1}$  ( $4.474$  and  $7.746\text{ }\mu\text{m}$ ) in these nonpolar ices. Similarly, the strongest  $O_3$  and  $CO_3$  bands are at about  $1039$  and  $2041\text{ cm}^{-1}$  ( $9.625$  and  $4.900\text{ }\mu\text{m}$ ), respectively. NO and  $NO_2$  might also be important as well. The strongest absorptions associated with these two species fall between  $1620$  and  $1610\text{ cm}^{-1}$  ( $6.17$ – $6.21\text{ }\mu\text{m}$ ) and near  $1860\text{ cm}^{-1}$  ( $5.38\text{ }\mu\text{m}$ ), respectively. Searching for these absorptions in appropriate *ISO* spectra will be important for understanding the chemistry in those regions and will provide important insight into the disposition of interstellar N and O. For example, the detection of these species along lines of sight probing quiescent regions of dense molecular clouds will support the hypothesis that photochemistry is important even in the densest regions of molecular clouds, while the nondetection would argue against this. It will also be important to probe lines of sight that are dominated by the protostellar environment such as represented by W33 A. Since the CO profile is not dominated by the nonpolar component in the spectrum of W33 A, one would anticipate that species such as  $N_2O$ ,  $O_3$ , and  $CO_3$  would not be as abundant with respect to the ice features associated with more polar, less volatile species such as  $H_2O$ , XCN,  $CH_3OH$ , and so on toward this object. Of course,  $N_2O$ ,  $O_3$ , and  $CO_3$ , if present in the gas, can freeze onto grains at temperatures above 30 K. Thus, band positions and profiles will be important diagnostic tools in sorting out the subtleties of the chemical processes at play in these very different environments. Further studies of nonpolar ice photochemistry will be warranted if *ISO* detects any of these photoproduct bands.

The production of  $CO_3$  in these experiments raises a question concerning the assignment of the weak  $2041\text{ cm}^{-1}$  ( $4.9\text{ }\mu\text{m}$ ) absorption detected toward W33 A (Larson et al. 1985; Geballe et al. 1985). Several suggestions have been put forward including  $C_3$ ,  $CH_3OH$ , and OCS. OCS has

been the most carefully considered in simulation experiments (Palumbo, Tielens, & Tokunaga 1995) which showed the best fit was provided by OCS frozen in CH<sub>3</sub>OH-rich ices. In light of the production of CO<sub>3</sub> in our experiments this too should be considered as a possible carrier. One might expect that if the 2041 cm<sup>-1</sup> interstellar band is due to CO<sub>3</sub>, its strength may correlate with the 2140 cm<sup>-1</sup> nonpolar component of the CO feature. In addition, if an object is found which possesses a significantly stronger 2041 cm<sup>-1</sup> feature, the assignment can be tested by searching for the other, weaker bands associated with these species. For CO<sub>3</sub> they fall at 1888 and 976 cm<sup>-1</sup> (5.3 and 10.2 μm), and for OCS they are near 860 and 520 cm<sup>-1</sup> (11.6 and 19.2 μm) (Hudgins et al. 1993).

Other important results of our photolysis studies are that (i) XCN was not formed in *any* of our experiments, and (ii) there are serious reservations concerning the detection of photoproducts that contain a *single* nitrogen atom. These are especially significant in light of the questions surrounding the identity and formation of the species designated XCN, a common photoproduct in laboratory ices containing a photolytic source of free N-atoms such as NH<sub>3</sub> (see d'Hendecourt et al. 1986; Bernstein et al. 1995). XCN is thought to be responsible for the interstellar 2165 cm<sup>-1</sup> band (Lacy et al. 1984). These experiments rule out the suggestion made in Teglar et al. (1995) that interstellar XCN is produced by the photolysis of N<sub>2</sub>-rich ices. Taken together, these results support the hypothesis made by Lacy et al. (1984) and Teglar et al. (1995) that XCN is somehow associated with the protostellar environment and is not a general characteristic of dense clouds. If this proves to be the case, careful characterization of the types of ices along lines of sight dominated by the protostellar environment versus those associated with more quiescent regions may well provide important constraints into the conditions prevalent in the early protosolar nebula.

## 6. SUMMARY

This paper presents the results of laboratory work in which the infrared spectral properties of CO frozen in mixed molecular ices containing O<sub>2</sub>, N<sub>2</sub>, CO<sub>2</sub>, and H<sub>2</sub>O were studied. The precise position, FWHM, and profile of the CO stretching fundamental near 2140 cm<sup>-1</sup> depends sensitively on the composition of the ice, the conditions under which it formed, and its subsequent thermal and radiation history. The optical constants (real and imaginary parts of the index of refraction) in the region of the solid CO feature are reported for several of the ices studied.

This project was undertaken to gain insight into the nature of the ices responsible for the 2140 cm<sup>-1</sup> interstellar, frozen CO feature which is characteristic of lines of sight through quiescent regions of dense molecular clouds. Comparison of the laboratory data with astronomical spectra show that CO frozen in O<sub>2</sub> and N<sub>2</sub> ices alone cannot account for the 2140 cm<sup>-1</sup> component. For N<sub>2</sub> and O<sub>2</sub>-rich ices, the feature is too narrow, the profile does not match, and the band falls at too low a frequency. Although mixtures containing comparable amounts of O<sub>2</sub>, N<sub>2</sub>, and CO do an excellent job of accounting for the low-frequency portion of the interstellar feature, they cannot reproduce the peak position or high-frequency side. The band is far too narrow if there is more than 2–3 times as much N<sub>2</sub> or O<sub>2</sub> as CO. The band position and width in the N<sub>2</sub>:O<sub>2</sub>:CO = 1:1:1 and 1:5:1 ices both produce narrow CO bandwidths,

and peak about 1 cm<sup>-1</sup> to the red of the interstellar feature. Thus, while N<sub>2</sub> and O<sub>2</sub> mixtures containing CO can contribute to the interstellar feature, an additional component is required to provide the high-frequency absorption. Of the nonpolar materials studied, CO<sub>2</sub> is the only one that produces the necessary high-frequency absorption. Concentration studies on four-component mixtures containing N<sub>2</sub>, O<sub>2</sub>, CO<sub>2</sub>, and CO show that the amount of CO<sub>2</sub> in the ice cannot exceed the amount of CO if a good fit to the interstellar 2140 cm<sup>-1</sup> CO feature is to be obtained. Of the ices we have studied, a composition of N<sub>2</sub>:O<sub>2</sub>:CO<sub>2</sub>:CO = 1:5:½:1 provided the best fit to the 2140 cm<sup>-1</sup> interstellar feature. This match is good both before and after UV photolysis and at all temperatures between 12 and 30 K.

While our experiments do not fully constrain the O<sub>2</sub> concentration needed in four-component nonpolar ices to provide a good match to the interstellar 2140 cm<sup>-1</sup> feature, the good fit provided by our N<sub>2</sub>:O<sub>2</sub>:CO<sub>2</sub>:CO = 1:5:½:1 ice allows us to make an estimate of how much material is tied up in the nonpolar ice component. Applying cosmic abundance constraints and assumed relative abundances of N<sub>2</sub>:O<sub>2</sub>:CO<sub>2</sub>:CO = 1:5:½:1, we find that between 15% and 70% (average = 35%) of the available interstellar N could be in the form of frozen N<sub>2</sub> along the lines of sight toward background stars, i.e., in the quiescent regions in clouds. This is reduced to about 1%–30% (average = 10%) for lines of sight toward embedded objects. Oxygen in the form of O<sub>2</sub> lies in the 1%–45% range (average = 20%) toward background sources and between 1% and 20% (average = 10%) toward embedded objects. The amount of oxygen tied up in frozen CO and CO<sub>2</sub> in nonpolar ices would then lie in the 2%–10% range toward background stars and between about 0.2% and 5% toward protostars. Similarly, between 3% and 13% of the carbon would then be tied up in frozen CO and CO<sub>2</sub> in nonpolar ices toward field stars, and 0.2%–6% toward embedded objects. These numbers imply that (i) most of the cosmic N is in the form of N<sub>2</sub>, (ii) in quiescent regions of dense clouds a significant fraction of the available O in the gas is in O<sub>2</sub>, and (iii) the ices surrounding embedded objects have a very different character from those found in quiescent regions.

Photolysis of a number of the ices produced a variety of new species including CO<sub>2</sub>, N<sub>2</sub>O, O<sub>3</sub>, CO<sub>3</sub>, HCO, H<sub>2</sub>CO, and possibly NO and NO<sub>2</sub>. The UV photolysis of N<sub>2</sub>-rich ices appears to be very inefficient at breaking N-N bonds and photolysis of these mixtures did *not* produce XCN. The identification of N<sub>2</sub>O, CO<sub>3</sub>, and O<sub>3</sub> among the common products of photolysis of ices containing O<sub>2</sub>, N<sub>2</sub>, CO<sub>2</sub>, and CO is important. It provides observers with new absorption bands to search for, bands whose presence or absence will place constraints on the conditions and chemistry occurring in dense clouds. Detection of interstellar solid N<sub>2</sub>O bands would indicate the presence of N<sub>2</sub>, while the strength of the O<sub>3</sub> bands would give an indication of the importance of O<sub>2</sub>.

We conclude this paper on the interstellar solid state CO feature by reiterating a point stressed nearly a decade ago. An observational resolution of one part of 10<sup>4</sup> is required to fully extract the information carried by this band, whereas one part in 10<sup>3</sup> is sufficient for most other interstellar ice features. The ability to measure the interstellar CO feature with such precision, in conjunction with the high sensitivity of the solid state CO band position and profile on the nature of the solid, makes it a powerful probe of the cloud (Allamandola & Sandford 1988).

We very gratefully acknowledge Max Bernstein for many helpful scientific discussions, help with laboratory procedures, and generously measuring all of the four-component ices reported here. We are also especially grateful to S. Laursen, Professor of Chemistry at Kalamazoo College, for her suggestion that Jamie Elsila carry out her Senior Research project with us at NASA/Ames, and for

her encouragement throughout this project. We also particularly thank P. Ehrenfreund, M. E. Palumbo, and G. Baratta for their comments and careful reading of the manuscript. As always, we also acknowledge Bob Walker for his excellent technical support. This work was supported by NASA grants 185-52-12-04 (Exobiology Program) and 452-33-93-03 (Origins of the Solar Systems Program).

## REFERENCES

- Allamandola, L. J., & Sandford, S. A. 1988, in *Dust in the Universe*, ed. M. E. Bailey & D. E. Williams (Cambridge: Cambridge Univ. Press), 229
- Allamandola, L. J., Sandford, S. A., & Valero, G. J. 1988, *Icarus*, 76, 225
- Bergmen, M. S., Schuh, D., Sceats, M. G., & Rice, S. A. 1978, *J. Chem. Phys.*, 69, 3477
- Bernstein, M. P., Sandford, S. A., Allamandola, L. J., Chang, S., & Scharberg, M. A. 1995, *ApJ*, 454, 327
- Bertie, J. E., Labbe, H. J., & Whalley, E. 1969, *J. Chem. Phys.*, 50, 4501
- Bohn, R. 1993, unpublished
- Bohn, R. B., Sandford, S. A., Allamandola, L. J., & Cruikshank, D. P. 1994, *Icarus*, 111, 151
- Cardelli, J. A., Meyer, D. M., Jura, M., & Savage, B. D. 1996, preprint
- Charnley, S. 1996, preprint
- Chiar, J. E., Adamson, A. J., Kerr, T. H., & Whittet, D. C. B. 1994, *ApJ*, 426, 240
- . 1995, *ApJ*, 455, 234
- Cruikshank, D. P., Roush, T. L., Owen, T. C., Geballe, T. R., DeBergh, C., Schmitt, B., Brown, R. H., & Bartholomew, M. J. 1993, *Science*, 261, 742
- d'Hendecourt, L. B., & Allamandola, L. J. 1986, *A&ASS*, 64, 453
- d'Hendecourt, L. B., Allamandola, L. J., & Greenberg, J. M. 1985, *A&A*, 152, 130
- d'Hendecourt, L. B., Allamandola, L. J., Grim, R. J. A., & Greenberg, J. M. 1986, *A&A*, 158, 119
- d'Hendecourt, L. B., & Jourdain de Muizon, M. 1989, *A&A*, 223, L5
- Dows, D. A. 1957, *J. Chem. Phys.*, 26, 745
- Dubost, H., Charneau, R., & Harig, M. 1982, *Chem. Phys.*, 69, 389
- Ehrenfreund, P., Breukers, R., d'Hendecourt, L., & Greenberg, J. M. 1992, *A&A*, 260, 431
- Eiroa, C., & Hodapp, K. W. 1989, *A&A*, 210, 345
- Ewing, G. E., Thompson, W. E., & Pimentel, G. C. 1960, *J. Chem. Phys.*, 32, 927
- Fately, W. G., Bent, H. A., & Crawford, B. 1959, *J. Chem. Phys.*, 31, 204
- Geballe, T. R. 1986, *A&A*, 162, 248
- Geballe, T. R., Baas, F., Greenberg, J. M., & Schutte, W. 1985, *A&A*, 146, L6
- Gerakines, P. A., Schutte, W. A., Greenberg, J. M., & van Dishoek, E. F. 1995, *A&A*, 296, 810
- Grundy, W. M., Schmitt, B., & Quirico, E. 1993, *Icarus*, 105, 254
- Hagen, W., Allamandola, L. J., & Greenberg, J. M. 1980, *A&A*, 86, L3
- Hagen, W., Tielens, A. G. G. M., & Greenberg, J. M. 1981, *Chem. Phys.*, 56, 367
- Hallam, H. E., & Scrimshaw, G. F. 1973, in *Vibrational Spectroscopy of Trapped Species*, ed. H. E. Hallam, (New York: Wiley), 11
- Herzberg, G. H. 1955, *Mem. Soc. Roy. Liege*, 15, 291
- Hudgins, D. M., Sandford, S. A., Allamandola, L. J., & Tielens, A. G. G. M. 1993, *ApJS*, 86, 713
- . 1994, *The AAS CD-ROM Series*, Vol. 1 (expanded version of the tables in *ApJS*, 86, 713)
- Jenniskens, P., Blake, D. H., Wilson, M. A., & Pohorille, A. 1995, *ApJ*, 455, 389
- Jewitt, D., Senay, M., & Matthews, H. 1996, *Science*, 271, 1110
- Jiang, G. J., Person, W. B., & Brown, K. G. 1975, *J. Chem. Phys.*, 62, 1201
- Kerr, T. H., Adamson, A. J., & Whittet, D. C. B. 1991, *MNRAS*, 251, 60P
- Lacy, J. H., Baas, F., Allamandola, L. J., Persson, S. E., McGregor, P. J., Lonsdale, C. J., Geballe, T. R., & van de Bult, C. E. P. M. 1984, *ApJ*, 276, 533
- Lacy, J. H., Carr, J., Evans, N., Baas, F., Achterman, J., & Arens, J. 1991, *ApJ*, 376, 556
- Latter, H. P., Davis, D. S., Black, J. H., & Fink, U. 1985, *ApJ*, 299, 873
- Latter, W. B., Radford, S. J. E., Jewell, P. R., Mangum, J., & Bally, J. 1996, ed. CO: Twenty-Five Years of Millimeter Wave Spectroscopy (Dordrecht: Kluwer)
- Leger, A., Gauthier, S., Défourneau, D., & Rouan, D. 1983, *A&A*, 117, 164
- Löwen, H. W., Bier, K. D., & Jodl, H. J. 1990, *J. Chem. Phys.*, 93, 8565
- Lucas, D., & Pimental, G. C. 1979, *J. Phys. Chem.*, 83, 2311
- Mathis, J. S. 1996, preprint
- Milligan, D. E., & Jacox, M. E. 1971, *J. Chem. Phys.*, 54, 927
- Mitchell, G. F., Allen, M., & Maillard, J. P. 1988, *ApJ*, 333, L55
- Mitchell, G. F., Maillard, J. P., Allen, M., Beer, R., & Belcourt, K. 1990, *ApJ*, 363, 554
- Moll, N. G., Clutter, D. R., & Thompson, W. E. 1960, *J. Chem. Phys.*, 45, 4469
- Owen, T. C., et al. 1993, *Science*, 261, 745
- Palumbo, M. E., & Strazzulla, G. 1993, *A&A*, 269, 568
- Palumbo, M. E., Tielens, A. G. G. M., & Tokunaga, A. T. 1995, *ApJ*, 449, 674
- Pearl, J., Ngoh, M., Ospina, M., & Khanna, R. 1991, *J. Geophys. Res.*, 96, 17477
- Pollack, J. B., Hollenbach, D., Beckwith, S., Simonelli, D., Roush, T., & Fong, W. 1994, *ApJ*, 421, 615
- Roux, J. A., Wood, B. E., Smith, A. M., & Plyler, R. R. 1980, *AEDC-TR-79-81 (AD-A088269)*
- St. Louis, R. V., & Crawford, B. 1965, *J. Chem. Phys.*, 42, 857
- Sandford, S. A. 1996a, *Meteoritics & Planetary Sci.*, 31, 449
- . 1996b, in *Polarimetry of the Interstellar Medium*, ed. W. Roberge & D. C. B. Whittet (Astron. Soc. Pac. Conf. Ser., Vol 97, San Francisco), 29
- Sandford, S. A., & Allamandola, L. J. 1990a, *Icarus*, 87, 188
- . 1990b, *ApJ*, 355, 357
- . 1993, *ApJ*, 417, 815
- Sandford, S. A., Allamandola, L. J., & Geballe, T. R. 1993, *Science*, 262, 400
- Sandford, S. A., Allamandola, L. J., Tielens, A. G. G. M., & Valero, G. J. 1988, *ApJ*, 329, 498
- Schmitt, B., Greenberg, J. M., & Grim, R. J. A. 1989, *ApJ*, 340, L33
- Schutte, W. A., Allamandola, L. J., & Sandford, S. A. 1993, *Icarus*, 104, 114
- Sekanina, Z. 1996, *A&A*, preprint
- Smith, A. L., Keller, W. E., & Johnston, H. L. 1950, *Phys. Rev.*, 79, 728
- Snow, T. P., & Witt, A. N. 1995, *Science*, 270, 1455
- Soifer, B. T., Puetter, R. C., Russell, R. W., Willner, S. P., Harvey, P. M., & Gillett, F. C. 1979, *ApJ*, 232, L53
- Tegler, S. C., Weintraub, D. A., Rettig, T. W., Pendleton, J., Whittet, D. B., & Kulesa, C. A. 1995, *ApJ*, 439, 279
- Tielens, A. G. G. M., & Hagen, W. 1982, *A&A*, 114, 245
- Tielens, A. G. G. M., Tokunaga, A. T., Geballe, T. R., & Baas, F. A. 1991, *ApJ*, 381, 181
- Tryka, K. A., Brown, R. H., & Anicich, V. 1995, *Icarus*, 116, 409
- Warren, S. G. 1986, *App. Optics*, 25, 2650
- Whittet, D. C. B. 1993, in *Dust and Chemistry in Astronomy*, ed. T. J. Millar & D. A. Williams (Cambridge: Cambridge Univ. Press), 9
- Whittet, D. C. B., Adamson, A. J., Duley, W. W., Geballe, T. R., & McFadzean, A. D. 1989, *MNRAS*, 241, 707
- Whittet, D. C. B., Longmore, A. J., & McFadzean, A. D. 1985, *MNRAS*, 216, 45p
- Whittet, D. C. B., et al. 1996, *ApJ*, 458, 363
- Wilson, R. W., Jefferts, K. B., & Penzias, A. A. 1971, *ApJ*, 161, L43
- Wood, B. E., & Roux, J. A. 1982, *J. Opt. Soc. Am.*, 72, 720

*Note added in proof.*—After submission of this paper we learned of two other related projects. P. Ehrenfreund et al. (*A&A*, 315, L341 [1996]) report the IR spectroscopy of mixed molecular ices containing similar compounds. The concentrations are complementary to those here, with CO generally the dominant species. M. E. Palumbo and G. Baratta (in preparation [1997]) are measuring the optical constants of *pure* molecular ices employing techniques such as simultaneous solutions for ices of different thicknesses,  $n_0$  determination, elimination of baseline corrections, etc. These techniques place additional constraints on the optical constants and should provide  $n$  and  $k$  values with very small uncertainties.